Research Square

Preprints are preliminary reports that have not undergone peer review.
They should not be considered conclusive, used to inform clinical practice,
or referenced by the media as validated information.

Fractal Geometry Meets Control Theory: Designing Motion through Rough Paths

Kistosil Fahim

fahim@its.ac.id

Institut Teknologi Sepuluh Nopember

Erika Hausenblas

Montanuniversität Leoben

Ben Goldys

The University of Sydney

Research Article

Keywords: Fractal drivers, Geometric control theory, Lie brackets, Nonlinear systems, Rough paths, Non-holonomic systems

Posted Date: November 25th, 2026

DOI: https://doi.org/10.21203/rs.3.rs-11743723/v1

License: This work is licensed under a Creative Commons Attribution 4.0 International License.
Read Full License

Additional Declarations: No competing interests reported.

Fractal Geometry Meets Control Theory: Designing Motion through Rough Paths

Kistosil Fahim[1*], Erika Hausenblas[2] and Ben Goldys[3]

[1*]Department of Mathematics, Institut Teknologi Sepuluh Nopember, Kampus ITS Sukolilo, Surabaya, 60111, Indonesia.
[2]Chair of Applied Mathematics, Montanuniversität Leoben, Peter-Tunner-Strasse 25/I, Leoben, 8700, Austria.
[3]School of Mathematics and Statistics, University of Sydney, Level 5, Carslaw Building F07, Sydney, NSW 2006, Australia.

*Corresponding author(s). E-mail(s): fahim@its.ac.id;
Contributing authors: erika.hausenblas@unileoben.ac.at;
beniamin.goldys@sydney.edu.au;

Abstract

This work develops a constructive framework for steering nonlinear non-holonomic control systems using fractal inputs. We employ explicit Koch-type paths with prescribed Hölder regularity and non-trivial Lévy areas to realise small-time motions along Lie bracket directions of control vector fields. In the rough path setting, such drivers are continuous but highly irregular; their iterated integrals directly encode the higher-order commutator effects usually approximated by oscillatory or impulsive controls. As model systems, we consider a unicycle and a car with one trailer and show that a short rough perturbation of duration τ can generate $O(\tau)$ displacements along second- and third-order Lie-bracket directions. The analysis combines the log-ODE expansion of rough differential equations with classical geometric controllability, providing a quantitative link between fractal geometry, signature calculus, and nonlinear control design.

Keywords: Fractal drivers, Geometric control theory, Lie brackets, Nonlinear systems, Rough paths, Non-holonomic systems

MSC Classification: 93B05 , 93C10 , 60L20 , 70F25 , 28A80 , 60L90 , 17B01

1 Introduction

Many mechanical systems, such as wheeled robots, cars with trailers and rolling bodies, are modelled by driftless control-affine systems

$$\dot{x}(t) = \sum_{i=1}^{m} u_i(t)\, V_i(x(t)), \qquad x(0) = x_0 \in \mathbb{R}^n, \tag{1.1}$$

with fewer inputs than states, $m < n$. At a state x, the admissible velocities span only the distribution $\Delta(x) = \operatorname{span}\{V_1(x), \dots, V_m(x)\}$. The missing directions are reached indirectly, through the Lie brackets $[V_i, V_j]$, $[V_i, [V_j, V_k]], \dots$ of the control vector fields. If these brackets span the tangent space, the system is locally controllable by the Chow–Rashevskii theorem, but it admits no continuous time-invariant stabilising feedback [1, 2]. Constructive steering methods therefore rely on open-loop manoeuvres: piecewise constant loops ("forward, turn, backwards, turn"), sinusoidal inputs [3], highly oscillatory controls [4, 5], or transverse functions [6].

All of these methods rely on the same mechanism. The net motion in a bracket direction is produced by the *iterated integrals* of the inputs. The motion along $[V_i, V_j]$ is produced by the signed area enclosed by the input loop, and the motion along higher brackets by higher iterated integrals. In this paper we take this observation as the starting point for design: we construct inputs by *prescribing their iterated integrals*. The natural language for this is the signature of a path and rough path theory [7–10]. The inputs we construct are self-similar (Koch-type) curves whose iterated integrals can be computed in closed form. Since the audience of this journal is not necessarily familiar with rough paths, we first recall the expansions for smooth inputs. Rough path theory then enters as the tool that keeps these expansions valid, with uniform error bounds, when the inputs become very irregular.

1.1 Iterated integrals and the Chen–Fliess expansion

Let $X_t^i = \int_0^t u_i(r)\, dr$ be the primitives of the inputs. We call $X = (X^1, \dots, X^m)$ the *driving path*; a closed loop of X corresponds to inputs with zero mean. For a word $I = (i_1, \dots, i_k)$ over the alphabet $\{1, \dots, m\}$ we set

$$X_{s,t}^I = \int_{s<r_1<\cdots<r_k<t} dX_{r_1}^{i_1} \cdots dX_{r_k}^{i_k}. \tag{1.2}$$

The collection of all these iterated integrals is called the *signature* $S_{s,t}$ of X over the interval $[s, t]$. It is decomposed into homogeneous levels.

$$X_{s,t}^{(k)} := \left(X_{s,t}^I\right)_{|I|=k} \in (\mathbb{R}^m)^{\otimes k}.$$

This denotes the k-th level of the signature. Level 1 contains the increments $X^i_t - X^i_s$, and level 2 the double integrals

$$X^{ij}_{s,t} = \int_{s<r_1<r_2<t} dX^i_{r_1}\, dX^j_{r_2} = \int_s^t \big(X^i_r - X^i_s\big)\, dX^j_r. \tag{1.3}$$

Applying the fundamental theorem of calculus repeatedly along the solution of (1.1) gives, for every smooth function $f : \mathbb{R}^n \to \mathbb{R}$, the *Chen–Fliess series* [11–13]

$$f(x_t) = \sum_{k\geq 0} \sum_{|I|=k} X^I_{s,t} \big(V_{i_1} V_{i_2} \cdots V_{i_k} f\big)(x_s) = f(x_s) + \sum_{k\geq 1} \sum_{|I|=k} X^I_{s,t} \big(V_{i_1} \cdots V_{i_k} f\big)(x_s). \tag{1.4}$$

Here each V_i acts as a first-order differential operator, $(V_i f)(x) = Df(x)\, V_i(x)$, and $V_{i_1} \cdots V_{i_k} f$ denotes the repeated application $V_{i_1}(V_{i_2}(\cdots(V_{i_k} f)))$. The term $k = 0$ corresponds to the word of length zero, for which we use the conventions $X^{\varnothing}_{s,t} = 1$ and $V_{\varnothing} f = f$; it contributes $f(x_s)$. Truncating after level N leaves a remainder of the size of the level-$(N+1)$ iterated integrals. Choosing for f the coordinate functions gives a Taylor-type expansion of the state increment in the iterated integrals of the input:

$$x_t - x_s = \sum_i X^i_{s,t}\, V_i(x_s) + \sum_{i,j} X^{ij}_{s,t} \big(DV_j\, V_i\big)(x_s) + \cdots \qquad . \tag{1.5}$$

This expansion contains all iterated integrals arising from the different combinations of the driving components. At the second level, these terms can be decomposed into symmetric and antisymmetric parts, with the antisymmetric component revealing the first Lie brackets. In particular, one gets

$$X^{ij}_{s,t} = \tfrac{1}{2} X^i_{s,t} X^j_{s,t} + \mathbb{A}^{ij}_{s,t}, \qquad \mathbb{A}^{ij}_{s,t} := \tfrac{1}{2}\big(X^{ij}_{s,t} - X^{ji}_{s,t}\big).$$

The symmetric part is fixed by integration by parts, $X^{ij} + X^{ji} = X^i X^j$. The antisymmetric part $\mathbb{A}^{ij}_{s,t}$ is the *Lévy area*: the signed area enclosed by the planar curve $r \mapsto (X^i_r, X^j_r)$, $r \in [s,t]$, after it has been closed by the straight segment from its end point (X^i_t, X^j_t) back to its starting point (X^i_s, X^j_s). Regions encircled counterclockwise count positively, those encircled clockwise negatively. Substituting the split into (1.5) gives

$$x_t - x_s = W(x_s) + \tfrac{1}{2}\big(DW\, W\big)(x_s) + \sum_{i<j} \mathbb{A}^{ij}_{s,t}\, [V_i, V_j](x_s) + \cdots, \tag{1.6}$$

where $W := \sum_i X^i_{s,t} V_i$ and $[V_i, V_j] = DV_j\, V_i - DV_i\, V_j$. The first two terms are the beginning of the Taylor expansion of the flow of the fixed vector field W, i.e. of the motion produced by the constant inputs $u_i \equiv X^i_{s,t}/(t-s)$; the trajectory of this flow is tangent to the distribution $\Delta(x) = \operatorname{span}\{V_1(x), \ldots, V_m(x)\}$ at every point. The area term is the part that cannot be produced by constant inputs. In particular, if the

driving path is a closed loop on $[s,t]$, i.e. $X^{(1)}_{s,t}=0$, then $W=0$ and we have

$$x_t - x_s = \sum_{i<j} \mathbb{A}^{ij}_{s,t}\,[V_i,V_j](x_s) + \big(\text{level-3 terms}\big). \tag{1.7}$$

This is the classical mechanism: a loop enclosing the area $\mathbb{A}$ moves the system by $\mathbb{A}$ along the bracket. If the loop encloses no area either, the second level vanishes completely and the leading term is of third order. For $m=2$ it reads (see Section 1.2)

$$x_t - x_s = X^{112}_{s,t}\,[V_1,[V_1,V_2]](x_s) - X^{122}_{s,t}\,[V_2,[V_1,V_2]](x_s) + \cdots. \tag{1.8}$$

This is the mechanism we use for the car with trailer in Section 4. At higher levels, the iterated integrals can be reorganized according to the corresponding nested Lie-bracket structure, giving rise to higher-order commutators.

1.2 The algebra behind the expansion

The signature satisfies two algebraic identities of different nature: one describes how it behaves when time intervals are concatenated, the other how products of its coefficients over the same interval decompose.

• *Chen's identity.* Fix $s<u<t$. Then the signature over $[s,t]$ is the product of the signatures over the two adjacent intervals $[s,u]$ and $[u,t]$:

$$S_{s,t} = S_{s,u}\otimes S_{u,t}, \quad \text{i.e.} \quad X^{(n)}_{s,t} = \sum_{k=0}^{n} X^{(k)}_{s,u}\otimes X^{(n-k)}_{u,t}, \qquad n\geq 0,$$

with $X^{(0)}\equiv 1$. Here $\otimes$ is the concatenation product in the tensor algebra $T((\mathbb{R}^m)) = \prod_{k\geq 0}(\mathbb{R}^m)^{\otimes k}$. The identity follows by splitting the domain of integration in (1.2) at u. The same concatenation identity also holds for iterated Itô integrals; however, their product algebra is governed by a quasi-shuffle rather than the ordinary shuffle identity. It is the tool behind the recursion for the iterated integrals of our self-similar curves in Section 3.

• *Shuffle identity.* Fix $s<t$ and two words I and J. Then the product of their iterated integrals over the same interval $[s,t]$ is a sum of iterated integrals of higher order,

$$X^{I}_{s,t}\,X^{J}_{s,t} = \sum_{K\in I \sqcup\!\sqcup J} X^{K}_{s,t},$$

where the sum runs over all *shuffles* (interleavings) of I and J, that is, all words of length $|I|+|J|$ obtained by merging the letters of I and J while preserving the relative order of the letters within each word. For one-letter words $I=(i)$, $J=(j)$ the shuffle identity reduces to $X^{i}_{s,t}X^{j}_{s,t} = X^{ij}_{s,t} + X^{ji}_{s,t}$, which is the integration-by-parts identity underlying the decomposition of the second level into its symmetric and antisymmetric parts. In tensor notation, this identity is equivalent to

$$\operatorname{Sym} X^{(2)}_{s,t} = \frac{1}{2}\,X^{(1)}_{s,t}\otimes X^{(1)}_{s,t}.$$

Hence the symmetric part of the second level is completely determined by the first level, while the new second-order information is contained in the antisymmetric part. The shuffle identity holds for smooth paths and, by closure, for geometric rough paths. For iterated Itô integrals, the ordinary shuffle identity is replaced by a quasi-shuffle relation involving quadratic-variation terms [14].

A consequence of the shuffle identity [11, 15] is that the logarithm

$$\ell_{s,t} := \log S_{s,t} = \sum_{n\geq 1} \frac{(-1)^{n-1}}{n} \, (S_{s,t} - 1)^{\otimes n}$$

is a Lie series. Written in a Hall basis of the free Lie algebra, it reads, up to level three,

$$\begin{aligned} \ell_{s,t} = \sum_{i=1}^{m} \ell_{s,t}^{i} \, e_i + \sum_{1\leq i<j\leq m} \ell_{s,t}^{[i,j]} \, [e_i, e_j] \\ + \sum_{1\leq i<j\leq m} \Big(\ell_{s,t}^{[i,[i,j]]} \, [e_i, [e_i, e_j]] + \ell_{s,t}^{[[i,j],j]} \, [[e_i, e_j], e_j] \Big) \\ + \sum_{1\leq i<j<k\leq m} \Big(\ell_{s,t}^{[i,[j,k]]} \, [e_i, [e_j, e_k]] + \ell_{s,t}^{[[i,k],j]} \, [[e_i, e_k], e_j] \Big) + \cdots \end{aligned} \tag{1.9}$$

where the dots stand for brackets of order at least four. The third level has dimension $(m^3 - m)/3$. For $m = 2$ it is spanned by $[e_1, [e_1, e_2]]$ and $[e_2, [e_1, e_2]] = -[[e_1, e_2], e_2]$, so that we have

$$\ell_{s,t} = \ell_{s,t}^{1} e_1 + \ell_{s,t}^{2} e_2 + \ell_{s,t}^{[1,2]} [e_1, e_2] + \ell_{s,t}^{1,(1,2)} [e_1, [e_1, e_2]] + \ell_{s,t}^{2,(1,2)} [e_2, [e_1, e_2]] + \cdots .$$

The coefficients follow from $\log S_{s,t} = (S_{s,t} - 1) - \frac{1}{2}(S_{s,t} - 1)^{\otimes 2} + \frac{1}{3}(S_{s,t} - 1)^{\otimes 3} - \cdots$ together with the shuffle identity:

$$\ell_{s,t}^{i} = X_{s,t}^{i}, \qquad \ell_{s,t}^{[1,2]} = \mathbb{A}_{s,t} = \tfrac{1}{2}\big(X_{s,t}^{12} - X_{s,t}^{21}\big),$$

and

$$\begin{aligned} \ell_{s,t}^{1,(1,2)} &= X_{s,t}^{112} - \tfrac{1}{2} X_{s,t}^{1} X_{s,t}^{12} + \tfrac{1}{12} \big(X_{s,t}^{1}\big)^2 X_{s,t}^{2} = \tfrac{1}{6}\big(X_{s,t}^{112} - 2X_{s,t}^{121} + X_{s,t}^{211}\big), \\ \ell_{s,t}^{2,(1,2)} &= -X_{s,t}^{122} + \tfrac{1}{2} X_{s,t}^{12} X_{s,t}^{2} - \tfrac{1}{12} X_{s,t}^{1} \big(X_{s,t}^{2}\big)^2 = -\tfrac{1}{6}\big(X_{s,t}^{122} - 2X_{s,t}^{212} + X_{s,t}^{221}\big). \end{aligned} \tag{1.10}$$

In particular, for a closed loop with vanishing area ($X_{s,t}^{(1)} = 0$, $\mathbb{A}_{s,t} = 0$) these reduce to $\ell_{s,t}^{1,(1,2)} = X_{s,t}^{112}$ and $\ell_{s,t}^{2,(1,2)} = -X_{s,t}^{122}$. The iterated brackets e_i, $[e_i, e_j]$, $[e_i, [e_j, e_k]], \ldots$ span the free Lie algebra but are linearly dependent because of the antisymmetricity and the Jacobi identity. A *Hall basis* is a standard choice of iterated Lie brackets forming a basis of the free Lie algebra [16, Ch. 4]. For $m = 2$, one possible Hall basis up to level three is e_1, e_2, $[e_1, e_2]$, $[e_1, [e_1, e_2]]$ and $[e_2, [e_1, e_2]]$. The coordinates $\ell_{s,t}^{I}$ of $\ell_{s,t}$ in this basis are called the *log-signature* coefficients. At level 1 they are

the increments, and at level 2 the Lévy areas, $\ell_{s,t}^{[i,j]} = \mathbb{A}_{s,t}^{ij}$. From level 3 onward, the coefficients are universal polynomials in the iterated integrals.[1] If $X_{s,t}^{(1)} = 0$ and $\mathbb{A}_{s,t} = 0$, then the shuffle identity gives $\operatorname{Sym} X_{s,t}^{(2)} = 0$, while $\mathbb{A}_{s,t} = 0$ eliminates the antisymmetric part. Hence $X_{s,t}^{(2)} = 0$, and consequently the level-3 part of $\ell_{s,t}$ is simply $X_{s,t}^{(3)}$. Expanding it in the basis $[e_1,[e_1,e_2]]$, $[e_2,[e_1,e_2]]$ gives the coefficients in (1.8). To interpret (1.4) algebraically, let $\mathcal{V}$ be the linear map that sends a word to the corresponding composition of differential operators,

$$\mathcal{V}(e_{i_1} \otimes \cdots \otimes e_{i_k}) = V_{i_1} V_{i_2} \cdots V_{i_k}, \qquad \mathcal{V}(1) = \mathrm{Id}.$$

Then (1.4) reads $f(x_t) = \big(\mathcal{V}(S_{s,t})f\big)(x_s)$. Concatenation of words corresponds to composition of operators, $\mathcal{V}(a \otimes b) = \mathcal{V}(a)\,\mathcal{V}(b)$. Hence $\mathcal{V}$ maps exponentials to exponentials and commutators to commutators; in particular $\mathcal{V}([e_i,e_j]) = V_iV_j - V_jV_i = [V_i,V_j]$, which is again a vector field, and more generally $\mathcal{V}(\ell_{s,t}) = \sum_I \ell_{s,t}^I V_I$ is a vector field, V_I denoting the iterated Lie bracket of vector fields associated with the Hall basis element indexed by I. Applying $\mathcal{V}$ to $S_{s,t} = \exp(\ell_{s,t})$ therefore gives, at least formally,

$$f(x_t) = \Big(\exp\big(\mathcal{V}(\ell_{s,t})\big) f\Big)(x_s), \qquad \mathcal{V}(\ell_{s,t}) = \sum_I \ell_{s,t}^I\, V_I. \tag{1.11}$$

Roughly speaking, over a short window, x_t is the time-one flow, started at x_s, of the *autonomous* vector field $\mathcal{V}(\ell_{s,t})$ [18–21]. Truncating $\ell_{s,t}$ at level N gives the *log-ODE method* [9, 19]:

$$\dot{z}_\rho = \sum_{|I| \le N} \ell_{s,t}^I\, V_I(z_\rho), \quad z_0 = x_s,\ \rho \in [0,1], \qquad x_t \approx z_1. \tag{1.12}$$

The coefficients are constant over the window, and the vector fields are evaluated along z_ρ, not frozen at x_s.

Expansions (1.5) and (1.12) carry the same information in different forms. The former expands the *state increment* in the signature and contains non-Lie terms such as $\frac{1}{2} DW\,W$. The latter expands the *generator of the flow* in the log-signature and contains Lie brackets only. For closed loops, $W = 0$, and both give (1.7) at leading order.

1.3 Why rough paths?

A key reason for using rough paths is their natural scaling behaviour. Compress a fixed driving loop X on $[0,1]$ into a window of length τ by setting $X_t^\tau = \tau^\alpha X_{t/\tau}$. This rescaling keeps the α-Hölder norm fixed, and the iterated integrals scale as

$$X_{0,\tau}^{\tau,(k)} = \tau^{k\alpha}\, X_{0,1}^{(k)}.$$

[1] For a group-like element, the logarithm is obtained by applying the first Eulerian idempotent. The first Eulerian and the normalized Dynkin idempotents agree in degrees 1 and 2, but in general differ from degree 3 onward; see [16, 17].

With bounded velocities ($\alpha = 1$), the area is $O(\tau^2)$, and so is the displacement along $[V_i, V_j]$. This agrees with the ball–box theorem of sub-Riemannian geometry [22, 23]: with bounded controls, the set of points reachable within time τ is comparable to a box with side lengths of order τ along the V_i, τ^2 along the brackets $[V_i, V_j]$, τ^3 along the brackets of third order, and so on. Now, in our setting, an $O(\tau)$ displacement along a second-order bracket within time τ requires $\alpha = 1/2$; along a third-order bracket it requires $\alpha = 1/3$. Keeping the α-Hölder norm fixed while $\tau \to 0$ means input velocities of order $\tau^{\alpha-1}$, which is unbounded. Piecewise constant loops with amplitude $\tau^{-1/2}$, fast sinusoids and fractal paths all belong to this regime, and their natural limit objects no longer have bounded variation.

In this regime, the expansions (1.5)–(1.12) must hold with error bounds that depend only on Hölder or p-variation norms of the iterated integrals, not on the velocities. For $\alpha \le 1/2$, the second level is no longer determined in general by the first-level path alone and must be supplied as part of the rough-path enhancement. Rough path theory provides exactly this. For a geometric p-rough path $\mathbf{X} = (X^{(1)}, \dots, X^{(\lfloor p \rfloor)})$, the equation $dx = \sum_i V_i(x)\, dX^i$ has a unique solution, provided $V_1, \dots, V_m \in C_b^\gamma(\mathbb{R}^n; \mathbb{R}^n)$ with $\gamma > p$; the log-ODE step has an error of order $\omega(s,t)^{(N+1)/p}$ (where $\omega(s,t)$ measures the p-variation of $\mathbf{X}$ on $[s,t]$, see Section 2, in particular (2.3)), and the solution depends continuously on $\mathbf{X}$ in the rough path metric (Lyons' universal limit theorem) [7, 9, 10]. For the design of a control, this has two consequences:

1. the implementable approximations, here the polygonal pre-fractals of finite refinement level, produce trajectories that converge to those of the ideal driver as soon as their rough path lifts converge;
2. the design is *robust in a precise sense*: perturbations of the input that are small in the rough path metric, i.e. including their areas, change the trajectory only slightly.

Equally important is what this robustness does not cover. Perturbations that are small in the supremum norm but carry a non-negligible area, such as small high-frequency loops, are *not* covered and do change the motion. Throughout the paper we use the word *robust* only in this rough path sense.

Finally, an area can be attached to any path abstractly, even to the constant path (a "pure area" rough path). Such an object, however, is not realised by any input. Our aim is the opposite: explicit inputs whose finite-level approximations can be implemented and whose iterated integrals are known in closed form.

1.4 Related work

The algebraic description of input–output maps by iterated integrals goes back to Chen [11] and Fliess [12, 13]. Its Lie-theoretic form was developed in the chronological calculus of Agrachev and Gamkrelidze [20], in Sussmann's product expansion [24], and in the work of Kawski and Sussmann [21]. Oscillatory and averaging methods [3–5], transverse functions [6] and measure-driven or impulsive frameworks [25–28] realise bracket motions with bounded-variation or singular inputs. Rough paths were connected with control early on [8]. More recent work addresses the inverse problem for

rough controlled equations [29], accessibility for geometric rough differential equations [30], rough flows [31] and stochastic control [32].

Closest to the present paper is the work of Nishimura and co-authors [33–36]. They use rough path analysis to justify inputs of unbounded variation and apply them to the stabilisation and linearisation of non-holonomic systems. In [36], one-dimensional rough signals are constructed whose first-level contribution vanishes in the limit while a symmetric second-level contribution survives. This produces the symmetrised terms $L_{g_i}g_j + L_{g_j}g_i$, analogous to Wong–Zakai corrections, and allows linearisation even when all Lie brackets vanish. The present work is complementary. We stay in the geometric setting, where, by the shuffle identity, the symmetric part of the second level is fixed by the first. For closed loops, therefore, all new directions come from Lie brackets, with the log-signature as coefficients. Our focus is on constructing explicit drivers that realise *prescribed* log-signature coefficients at levels 2 and 3.

1.5 Contributions and organisation

1. We introduce generalised Koch-type curves, determined by a motif of segment lengths r_k and angles a_k. Their Hölder exponent is $\alpha = \log(1/r_{\max})/\log M$. The Lévy area of the level-n polygon satisfies the affine recursion $A_{n+1} = \rho A_n + A_1$ with $\rho = \sum_k r_k^2$. When $\rho < 1$ the areas converge geometrically, and the limit area is an explicit function of the motif parameters, which we invert to prescribe the area at $\alpha = 1/2$ (Section 3).
2. We prove that the rough path lifts of the polygonal pre-fractals converge geometrically, with a rate explicit in the motif (Theorem 1), and we derive an explicit bound on the steering error of the implementable, piecewise constant inputs (Corollary 2).
3. We extend the construction to level 3: motifs with vanishing increment and vanishing area but a prescribed coefficient $\ell^{1,(1,2)}$ at $\alpha = 1/3$. We apply it to the car with trailer, whose hitch direction at the origin is reached only through third-order brackets (Section 4).
4. We illustrate both constructions on the unicycle and the car with trailer, and confirm the predicted displacements and convergence rates by simulations of the pre-fractal inputs (Example 3.4 and Example 4.2).

Section 2 collects the control-theoretic and rough path background, Section 3 contains the construction of the Koch-type controls, Section 4 treats higher-level constructions and their application to a car with one trailer, while Section 5 presents the conclusions and outlook. Appendices A and B contain short introductions to rough path theory and nonlinear control theory, respectively.

2 Preliminaries: Control Theory, Rough Paths, and Non-holonomic Systems

We briefly summarise the notions needed in the sequel, in particular the concepts of reachable sets and the Lie algebra rank condition (LARC)/Chow–Rashevskii theorem,

the rough-path enhancement $(X, \mathbb{X}, \ldots)$, the log–ODE expansion, and standard non-holonomic models together with their Lie–bracket structure.

2.1 Control-theoretic background

We collect the geometric control notions that explain why *Lie brackets* govern small-time motion and local reachability. First, for completeness, we define the Lie bracket.

Definition 1 (Lie bracket of vector fields)**.** Let V_1, V_2 be two smooth vector fields on a manifold M (for simplicity, $M \subset \mathbb{R}^n$). The *Lie bracket* of V_1 and V_2 is the vector field

$$[V_1, V_2](x) := J_{V_2}(x) \cdot V_1(x) - J_{V_1}(x) \cdot V_2(x),$$

where $J_{V_j}(x)$ denotes the Jacobian matrix of V_j at x, $j = 1, 2$. So, the Lie bracket measures the noncommutativity of the differential operators V_1 and V_2.

Consider a control-affine system on a smooth manifold $M \subset \mathbb{R}^n$,

$$\dot{x}(t) \;=\; V_0(x(t)) \;+\; \sum_{i=1}^{m} u_i(t)\, V_i(x(t)), \qquad x(0) = x_0, \tag{2.1}$$

with drift V_0 and control vector fields $V_1, \ldots, V_m$. At a state $x(t)$, $t \geq 0$, the *instantaneous control directions* are the vectors $(V_1(x), V_2(x), \cdots, V_m(x))$, $x = x(t)$; for example, by switching inputs rapidly, one can also generate motion along *Lie brackets* of the V_i, $i = 1, \cdots, m$.

We focus primarily on non-holonomic systems, in particular the unicycle model and the car-with-trailer system, which serve as typical examples of driftless control-affine systems. A kinematic unicycle is a straightforward mathematical representation of a vehicle with a single wheel that is capable of moving forward or backwards and turning by changing its orientation. However, this unicycle cannot move directly sideways; any lateral displacement has to be achieved by combining forward motion with rotation.

Example 2.1. *A* ***unicycle*** *has the state $x = (x_1, x_2, x_3)$, where (x_1, x_2) represents its position in the plane and $x_3 = \theta$ denotes its heading (the direction in which the wheel points). We assume the wheel* rolls without slipping*: it can move* forward or backward *along its heading and can* rotate in place*, but it cannot instantaneously slide sideways.*

Two scalar inputs $u = (u_1, u_2)$ encode these actions:

$$\dot{x}_1(t) = u_1(t) \cos x_3(t), \quad \dot{x}_2(t) = u_1(t) \sin x_3(t),$$
$$\dot{x}_3(t) = u_2(t), \quad x(0) = x_0 \in \mathbb{R}^3.$$

Here

- *u_1 is the* forward speed *along the current heading $x_3 = \theta$;*
- *u_2 is the* turn rate *(angular velocity).*

The third equation says turning does not change (x_1, x_2) directly; the first two say that forward motion projects onto the axes according to the current heading. One can write the system in the control-affine form $\dot{x}(t) = u_1 V_1(x(t)) + u_2 V_2(x(t))$, with

$$V_1(x) = \begin{bmatrix} \cos x_3 \\ \sin x_3 \\ 0 \end{bmatrix}, \qquad V_2(x) = \begin{bmatrix} 0 \\ 0 \\ 1 \end{bmatrix}.$$

There is no absolutely continuous input that instantaneously moves the unicycle sideways. This is the non-holonomic *nature of the model.*

2.1.1 Reachability and Controllability

In a controlled system, we are interested in the set of points reachable from a given initial state. More precisely, let $\mathcal{R}^+(x_0, T)$ denote the set of states reachable from x_0 in time less than T by admissible inputs. The system is said to be *locally accessible* at x_0 if

$$\operatorname{int} \mathcal{R}^+(x_0, T) \neq \varnothing$$

for all sufficiently small $T > 0$. It is said to be *small-time locally controllable (STLC)* at x_0 if, for all small $T > 0$, every point in a neighbourhood of x_0 is both forward- and backward-reachable within time T.

Having introduced the concept of reachable sets, we now turn to the question of how to *characterise* these sets in terms of the system's vector fields. While the reachable set $\mathcal{R}^+(x_0, T)$ captures all points that can be attained through admissible inputs within time T, its structure is deeply influenced by the geometry of the underlying control directions. In particular, the directions generated not only by the control vector fields themselves but also by their *iterated Lie brackets* determine the local accessibility of the system.

Let $\operatorname{Lie}\{V_1, \ldots, V_m\}$ be the smallest Lie algebra of vector fields containing $V_1, \ldots, V_m$ (closed under linear combinations and brackets). Its *evaluation* at x is

$$\operatorname{Lie}(x) \;:=\; \operatorname{span}\{\, W(x) :\; W \in \operatorname{Lie}\{V_1, \ldots, V_m\} \,\} \;\subseteq\; T_x M.$$

This idea is formalised by the Lie Algebra Rank Condition (LARC); see Appendix B, Definition 7.

Returning to Example 2.1, one finds that at every state the three vectors

$$V_1(x) = \begin{bmatrix} \cos x_3 \\ \sin x_3 \\ 0 \end{bmatrix}, \quad V_2(x) = \begin{bmatrix} 0 \\ 0 \\ 1 \end{bmatrix}, \qquad [V_1, V_2](x) = \begin{bmatrix} \sin x_3 \\ -\cos x_3 \\ 0 \end{bmatrix} \tag{2.2}$$

form an orthonormal basis of $\mathbb{R}^3$ at every x (V_1 and $[V_1, V_2]$ are orthogonal unit vectors in the plane, V_2 points in the x_3-direction), so that

$$\operatorname{span}\{V_1(x), V_2(x), [V_1, V_2](x)\} = \mathbb{R}^3, \quad x \in \mathbb{R}^3.$$

This shows that the Lie algebra generated by $\{V_1, V_2\}$ has full rank everywhere on M, and hence the unicycle satisfies the LARC. By the Chow–Rashevskii theorem, this implies that the unicycle can reach any nearby configuration. To make the geometric structure explicit, let us write $V_0 \equiv 0$. The control vector fields $V_1, \dots, V_m$ assign to each point x a set of tangent directions $V_i(x) \in T_x\mathbb{R}^n$. The pointwise linear span

$$\Delta(x) \coloneqq \operatorname{span}\{V_1(x), \dots, V_m(x)\} \subseteq T_x\mathbb{R}^n$$

is called the *distribution* generated by the control vector fields; it collects the directions in which the system can move *instantaneously*.

In general, Δ need not be integrable: additional directions may be reachable only through iterated commutators of the vector fields. The smallest distribution that contains all Lie brackets of $V_1, \dots, V_m$ is the *bracket-generated* distribution, (sometimes called Chow-distribution)

$$\Delta^{\infty}(x) \coloneqq \operatorname{span}\{W(x) : W \in \operatorname{Lie}_x(V_1, \dots, V_m)\},$$

where $\operatorname{Lie}_x(V_1, \dots, V_m)$ denotes the Lie algebra generated by the control vector fields at x. When $\Delta^{\infty}(x) = T_x\mathbb{R}^n$, the system is locally controllable at x by the Chow–Rashevskii theorem, see Appendix B, Theorem 2.

A practical question is: how can one design a control that makes the unicycle at $(0,0,0)^{\top}$ move sideways in the direction of $[V_1, V_2](0)$? One approach is to construct *loops* in the control plane, which produce a net sideways shift due to the noncommutativity of the forward and turning motions, see [37, p. 130]. Fix a small duration $\tau > 0$ and amplitudes $a, b \in \mathbb{R}$, $a, b \sim 1/\sqrt{\tau}$. Apply the four pulses

$$u_1(t) = \begin{cases} a, & t \in [0, \frac{\tau}{4}], \\ -a, & t \in (\frac{2\tau}{4}, \frac{3\tau}{4}], \\ 0, & \text{otherwise}, \end{cases} \qquad \text{and} \qquad u_2(t) = \begin{cases} b, & t \in [\frac{\tau}{4}, \frac{2\tau}{4}], \\ -b, & t \in (\frac{3\tau}{4}, \tau], \\ 0 & \text{otherwise}. \end{cases}$$

This sequence corresponds (for the unicycle) to "forward, then turn, then backwards, then turn". Note that the loop has zero mean,

$$\int_0^{\tau} u_1(t)\, dt = \int_0^{\tau} u_2(t)\, dt = 0,$$

but *nonzero* signed Lévy area[2] in the (v_1, v_2)-plane, where $v_i(t) = \int_0^t u_i(s)\, ds$:

$$\mathbb{A} = \frac{1}{2} \int_0^{\tau} \int_0^{s} [dv_1(t)\, dv_2(s) - dv_2(t)\, dv_1(s)] = \tfrac{1}{16} ab\, \tau^2.$$

[2] see (A4).

By the Baker–Campbell–Hausdorff (BCH) expansion (equivalently, the step–2 log–ODE for rough/oscillatory inputs), the resulting state increment is, to leading order,

$$\Delta x = \mathbb{A}\,[V_1, V_2](x_0) + O\big((|a| + |b|)^3\tau^3\big) = \frac{ab\,\tau^2}{16}\,[V_1, V_2](x_0) + O\big((|a| + |b|)^3\tau^3\big),$$

because the increments of the loop vanish, so that the non-Lie term $\frac{1}{2}DW\,W$ in (1.6) is absent (Corollary 1). For the unicycle, the vector fields V_1, V_2 and the bracket $[V_1, V_2]$ were computed in (2.2). Since $[V_1, V_2](x)$ is orthogonal to the heading direction $(\cos x_3, \sin x_3)$, the net displacement produced by the area term is *sideways*, i.e. perpendicular to the current heading. The sign of $\mathbb{A}$ depends on the loop orientation (order of the pulses). However, to obtain a shift of order τ, one must choose amplitudes a, b of order $\tau^{-1/2}$; these become unbounded as $\tau \downarrow 0$, i.e. in the limit one obtains a singular control [3]. For instance, $a = b = \tau^{-1/2}$ gives $\mathbb{A} = \tau/16$ and a remainder $O(\tau^{3/2})$.

Alternatively, one may construct a *sinusoidal (averaging) loop*, as in Sussmann and Liu [4] or Murray and Sastry [3], given for example by

$$u_1(t) = \varepsilon\cos(\omega t), \qquad u_2(t) = \varepsilon\sin(\omega t), \qquad t \in [0, 2\pi/\omega].$$

Over one period, both means vanish,

$$\int_0^{2\pi/\omega} u_i(t)\,dt = 0, \quad i = 1, 2,$$

but the signed Lévy area over one period is nonzero:

$$\mathbb{A} = \frac{1}{2}\int_0^{2\pi/\omega}\int_0^{s} \big[dv_1(t)\,dv_2(s) - dv_2(t)\,dv_1(s)\big] = \frac{\pi}{\omega^2}\varepsilon^2,$$

where $v_i(t) = \int_0^t u_i(s)\,ds$. Hence, the loop produces an averaged lateral displacement of order ε^2/ω^2 per period, i.e. a drift of order ε^2/ω per unit time. Higher harmonics or phase shifts can be used to scale and reorient the resulting displacement.

Despite their elegance, sinusoidal or averaging-based loops have several well-known limitations in practice and in numerical implementation. First, the averaging approximation assumes a clear separation of time scales (ω large), which can require unrealistically high-frequency actuation and leads to numerical stiffness in simulation (see Bullo and Lewis [40, Chapter 9], Choset et al. [41]). Second, in motion planning, such oscillatory inputs may excite unmodeled dynamics (e.g., actuator saturation, slip, or delays) and are sensitive to phase and timing errors (Sontag [38], Murray and Sastry [3]). Finally, since the averaged drift appears only at order ε^2/ω, these methods often require long execution times or precise synchronisation to achieve noticeable displacements, limiting their efficiency in real-time or energy-constrained applications (see also Agrachev and Sachkov [42]).

[3] For the definition of singular or nonsingular controls, see Sontag [38, p. 152] or [39].

In contrast, rough path theory permits the use of *fractal loops*, which are defined on arbitrary time intervals and possess only limited regularity. In this rough-path framework, one can interpret and solve the differential equation directly in the rough sense. Thus rough path theory allows us to treat irregular inputs such as a Koch-type fractal with Hölder exponent $\alpha = 1/2$. If the driving loop is compressed into a short window $[0, \tau]$ as in Section 1, and its increment vanishes, $X^{(1)}_{0,\tau} = 0$, then by Corollary 1

$$\Delta x \;=\; \sum_{i<j} \mathbb{A}^{ij}_{0,\tau}\, [V_i, V_j](x_0) \;+\; O(\tau^{3/2}),$$

where $\mathbb{A}^{ij}_{0,\tau} = \frac{1}{2}(X^{ij}_{0,\tau} - X^{ji}_{0,\tau})$ is the Lévy area of the driving path. A loop with prescribed area $\mathbb{A}^{12}_{0,\tau} = \mathbb{A} \sim \tau$ therefore produces a *pure* bracket step of size $\mathbb{A}$ along $[V_1, V_2]$, i.e. a clean sideways slide.

2.2 Rough path analysis

Our motivation for using fractal inputs is that Lie-bracket motion can be encoded directly in their iterated integrals. Rough path theory provides the natural framework for analysing such irregular drivers and the resulting controlled dynamics. However, to make sense of controlled dynamics

$$\mathrm{d}x_t \;=\; \sum_{i=1}^{m} V_i(x_t)\, \mathrm{d}X^i_t,$$

we need a calculus that predicts *how the system moves* when the input path $\mathbf{X} = (X^1, \dots, X^m)$ is a fractal. The central idea of Lyons' rough path theory is to enhance $\mathbf{X}$ with additional information, namely its *iterated integrals*. The reward is a robust, purely pathwise solution theory with clean expansions that explain bracket effects. For a smooth driver, Section 1 gives two equivalent descriptions of the local behaviour of the solution. The Taylor expansion (1.5) expresses the *increment* $x_t - x_s$ in the signature of X. Its second-order term contains the full second level $X^{(2)}_{s,t}$, and Lie brackets appear only after the symmetric part $\frac{1}{2}X^{(1)}_{s,t} \otimes X^{(1)}_{s,t}$ has been separated off; see (1.6); the remaining term $1/2(DW\,W)(x_s)$ is not a Lie bracket and vanishes precisely for closed loops, i.e., if $X^{(1)}_{s,t} = 0$. The log-ODE (1.12), in contrast, describes the *generator* of the flow and contains Lie brackets only, with the log-signature as coefficients.

In both descriptions, all coefficients are iterated integrals of X or polynomials in them. For $X \in \mathcal{C}^1$ they are classical Riemann–Stieltjes integrals, and by Young's theory [43] they remain well defined as limits of Riemann sums if X is Hölder continuous with exponent $\alpha > 1/2$. For $\alpha \le 1/2$ this breaks down already at level two: the increments $X^{(1)}_{s,t}$ are still well defined, but the second level, and in particular the Lévy area, is no longer determined by the path. Different smooth approximations of the same path may produce different areas in the limit. For instance, adding to a path smaller and smaller loops that all enclose the same total area changes neither the path nor its increments in the limit, but shifts $\mathbb{A}_{s,t}$ by that area. The area therefore has to be *prescribed* as

additional information, and for $\alpha \leq 1/3$ the same holds for the third level. A rough path is precisely a path together with this information. For the reader's convenience, the definitions of signature levels and geometric rough paths are recalled below from Appendix A. Let us introduce the definition for iterated integrals and signature levels.

Definition 2. Let $\mathbf{X} : [0,1] \to \mathbb{R}^m$ be a path. Its *iterated integrals* on an interval $[s,t]$ are the tensors given by

$$X_{s,t}^{(k)} = \int_{s<u_1<\cdots<u_k<t} \mathrm{d}X_{u_1} \otimes \cdots \otimes \mathrm{d}X_{u_k},\ k = 1, 2, \ldots$$

For a two-dimensional path $X = (X^1, X^2)$, the second level of its signature is

$$X_{s,t}^{(2)} = \int_{s<u_1<u_2<t} dX_{u_1} \otimes dX_{u_2} \in \mathbb{R}^2 \otimes \mathbb{R}^2.$$

The coordinate entries are defined by

$$X_{s,t}^{(2),ij} := \int_{s<u_1<u_2<t} dX_{u_1}^i \, dX_{u_2}^j, \qquad i,j \in \{1,2\}.$$

The Lévy area is the antisymmetric part given by

$$\mathbb{A}_{s,t}^{i,j} := \ell_{s,t}^{[i,j]} = \tfrac{1}{2}\big(X_{s,t}^{(2),ij} - X_{s,t}^{(2),ji}\big).$$

For a small "rectangle loop" (right, up, left, down) of side lengths a, b we get $\mathbb{A} = a\,b$ with a sign given by orientation. Even when the path is jagged (Koch, Brownian), the area *is* the right second-order datum that determines sideways (bracket) motion. For smooth $\mathbf{X}$ these iterated integrals are well-defined and satisfy *Chen's relation*:

$$X_{s,t}^{(k)} = \sum_{\ell=0}^{k} X_{s,u}^{(\ell)} \otimes X_{u,t}^{(k-\ell)} \quad \text{for all } s < u < t.$$

At level 2 this reads

$$X_{s,t}^{(2),ij} = X_{s,u}^{(2),ij} + X_{u,t}^{(2),ij} + X_{s,u}^{(1),i} X_{u,t}^{(1),j},$$

and, by antisymmetrisation,

$$\mathbb{A}_{s,t}^{ij} = \mathbb{A}_{s,u}^{ij} + \mathbb{A}_{u,t}^{ij} + \frac{1}{2}\big(X_{s,u}^{(1),i} X_{u,t}^{(1),j} - X_{s,u}^{(1),j} X_{u,t}^{(1),i}\big).$$

Next we recall the notion of a geometric p-rough path; the p-variation is defined in (A2).

Definition 3 (Geometric p-rough path)**.** Fix $p \in [1, \infty)$. A *geometric p-rough path* over $\mathbb{R}^m$ is a collection

$$\mathbf{X} = (X^{(1)}, X^{(2)}, \dots, X^{(N)}), \qquad N = \lfloor p \rfloor,$$

of (generalised) iterated integrals up to level N that (i) satisfy Chen's relation, (ii) have finite p-variation/Hölder control consistent with their level (level-k behaves like (size)^k), and (iii) arise as limits of signatures of smooth paths (the geometricity condition).

A p-rough path remembers enough of the "multiplicative" features of X (first $N = \lfloor p \rfloor$ levels) so that controlled ODEs driven by X make pathwise sense. If X is α-Hölder, then one may take $p = 1/\alpha$, and

$$\begin{aligned} \alpha \in (\tfrac{1}{3}, \tfrac{1}{2}] &\Rightarrow p \in [2, 3) \quad \text{(need levels 1 and 2)}, \\ \alpha \in (\tfrac{1}{4}, \tfrac{1}{3}] &\Rightarrow p \in [3, 4) \quad \text{(need levels } 1, 2, 3). \end{aligned}$$

This means that to obtain higher-order Lie brackets, one needs rougher inputs (smaller α).

Let us turn our attention to rough differential equations (RDEs). Given vector fields $V_1, \dots, V_m$ and a geometric p-rough path $\mathbf{X} = (X^{(1)}, X^{(2)}, \dots, X^{(N)})$ over $\mathbb{R}^m$, Lyons' theory defines a unique *RDE solution*

$$\mathrm{d}x_t \;=\; \sum_{i=1}^{m} V_i(x_t)\, \mathrm{d}\mathbf{X}_t^i, \qquad x_0 \in \mathbb{R}^n,$$

as the limit of solutions driven by smooth approximations whose signatures converge to $\mathbf{X}$.

Let $p \geq 1$, $N = \lfloor p \rfloor$, and let $\mathbf{X}$ be a geometric p-rough path over $\mathbb{R}^m$. We measure the size of $\mathbf{X}$ on $[s, t]$ by the *p-variation*[4]

$$\omega(s, t) \;:=\; \|\mathbf{X}\|_{p\text{-var};[s,t]}^{p}. \tag{2.3}$$

Now, we can state our next proposition.

Proposition 1 (Log-ODE method, cf. [9, Ch. 10], [19])**.** Let $p \geq 1$, $N = \lfloor p \rfloor$, and let $\mathbf{X}$ be a geometric p-rough path over $\mathbb{R}^m$. Let $V_1, \dots, V_m \in C_b^{\gamma}(\mathbb{R}^n; \mathbb{R}^n)$ with $\gamma > p$, and let x be the solution of $dx_t = \sum_i V_i(x_t)\, dX_t^i$. For $s < t$ let $\ell_{s,t} = \sum_{|I| \leq N} \ell_{s,t}^I e_I$ be the log-signature of $\mathbf{X}$ on $[s, t]$, expanded in a Hall basis (e_I), and let z^s solve

$$\dot{z}_\rho^{\,s} = \sum_{|I| \leq N} \ell_{s,t}^I\, V_I\big(z_\rho^{\,s}\big), \qquad z_0^{\,s} = x_s, \quad \rho \in [0, 1], \tag{2.4}$$

[4] In the rough path literature ω is called a *control*; we avoid this term to prevent confusion with control inputs.

where V_I is the iterated Lie bracket of vector fields corresponding to e_I. Then, there exists a constant C, depending only on p, γ and $\|V\|_{C_b^\gamma}$, such that

$$\left|x_t - z_1^s\right| \le C\,\omega(s,t)^{(N+1)/p} \qquad \text{whenever } \omega(s,t) \le 1.$$

For $p \in [2,3)$, i.e. $N = 2$, equation (2.4) reads

$$\dot{z}_\rho^{\,s} = \sum_i X_{s,t}^i\, V_i(z_\rho^s) + \sum_{i<j} \mathbb{A}_{s,t}^{ij}\,[V_i, V_j](z_\rho^s), \qquad z_0^s = x_s.$$

Three important features of Proposition 1 should be mentioned: The coefficients $\ell_{s,t}^I$ are *constants*, computed over the whole interval $[s,t]$; the vector fields are evaluated *along* the auxiliary trajectory z_ρ^s and not frozen at x_s; and the conclusion is that the flow map $\Phi_{s,t} : x_s \mapsto x_t$ is approximated by the time-one map $\exp(\mathcal{V}(\ell_{s,t}))$. In particular, the statement that $\log \Phi_{s,t}$ is a Lie series concerns the *generator* of the flow, and the generator acts through the exponential,

$$\exp(W)(x_s) - x_s = W(x_s) + \tfrac{1}{2}(DW\,W)(x_s) + \cdots,$$

so the increment $x_t - x_s$ is *not* a combination of Lie-bracket terms only; this is consistent with (1.5)–(1.6). What we use in the sequel is the following consequence, in which the non-Lie terms disappear because the driver is constructed to be a loop.

Corollary 1. Let $X_{s,t}^{(1)} = 0$.

(a) If $p \in [2,3)$, then $W \equiv 0$ in (1.6) and

$$x_t - x_s = \sum_{i<j} \mathbb{A}_{s,t}^{ij}\,[V_i, V_j](x_s) + O\big(\omega(s,t)^{3/p}\big).$$

(b) If $p \in [3,4)$, $m = 2$ and $\mathbb{A}_{s,t}^{12} = 0$, then, with the coefficients (1.10), which here reduce to $\ell_{s,t}^{1,(1,2)} = X_{s,t}^{112}$ and $\ell_{s,t}^{2,(1,2)} = -X_{s,t}^{122}$,

$$x_t - x_s = \ell_{s,t}^{1,(1,2)}[V_1,[V_1,V_2]](x_s) + \ell_{s,t}^{2,(1,2)}[V_2,[V_1,V_2]](x_s) + O\big(\omega(s,t)^{4/p}\big).$$

Observe:

- Level 1 increments $X^{(1)}$ create motion along the *base* vector fields V_i (first-order motion).
- Level 2 increments contribute through their antisymmetric part $\mathbb{A}_{s,t}$ (the Lévy area), which creates motion along *brackets* $[V_i, V_j]$ (second-order bracket motion).
- One can define higher levels which create a motion along higher brackets $[V_i,[V_j,V_k]]$, $1 \le i,j,k \le m$.

This is why any input whose driving path encloses area (smooth, oscillatory or fractal) can access directions that have no direct actuator; what distinguishes rough inputs is

the *scaling* of these contributions: Compress a fixed rough pattern to a time window of length τ. If X is α-Hölder, the level-k signature scales like $\tau^{k\alpha}$:

$$\text{level } 1 \sim \tau^{\alpha}, \quad \text{level } 2 \sim \tau^{2\alpha}, \quad \dots, \quad \text{level } N \sim \tau^{N\alpha}.$$

In the setting of Example 3.3, the two control vector fields V_1 (forward motion) and V_2 (turning) generate, through their Lie bracket, all directions in $\mathbb{R}^3$. More precisely,

$$\operatorname{span}\{V_1(x), V_2(x), [V_1, V_2](x)\} = \mathbb{R}^3, \qquad x \in \mathbb{R}^3.$$

Thus, although the unicycle cannot move instantaneously in the lateral direction, this missing direction is generated by the Lie bracket $[V_1, V_2]$. A rough driving signal with nonzero Lévy area can produce a net displacement in this bracket direction even when its first-level increments vanish, that is, when the driving path forms a closed loop. Koch-type inputs provide an explicit way of constructing such closed loops with prescribed Lévy area and therefore of generating a controlled motion in the direction $[V_1, V_2]$.

3 The Implementation of a Koch-type Control

Our aim in this section is to construct Koch-type curves with prescribed Hölder regularity and prescribed signature data. We introduce a class of generalised Koch-type curves and then explain how the motif parameters can be chosen to realise the desired regularity and, at level 2, a prescribed Lévy area.

3.1 The Construction of a generalised Koch-type Fractal

A Koch-type curve is described by a motif, which is a small polygonal path whose chord has length 1, specified by relative segment lengths and turning angles. Iteratively replacing each straight segment with the motif generates the full fractal (like the Koch curve). To be mathematically precise, we give the exact definition.

Definition 4. A *motif* is the basic building block of a self-similar fractal curve. It consists of a finite sequence of M straight-line segments, each characterised by a *relative length* $r_k > 0$ and a *turning angle* a_k, measured from the horizontal direction, $k = 1, \cdots, M$. The associated vectors are

$$v_k = r_k(\cos a_k, \sin a_k)^{\top}, \qquad k = 1, \dots, M, \tag{3.1}$$

placed tip-to-tail to form a small geometric "bump" or pattern. The motif starts at the origin and ends at a point one unit away, satisfying the *unit chord condition*

$$\sum_{k=1}^{M} v_k = (1, 0)^{\top}. \tag{3.2}$$

In addition, we impose the contraction condition $0 < r_k < 1$ for all $k = 1, \ldots, M$. For the nonzero-area construction at level 2 we further require

$$\rho_2 := \sum_{k=1}^{M} r_k^2 < 1,$$

which ensures convergence of the Lévy areas of the polygonal approximations; see Lemma 1 and Remark 2. The zero-area level-3 construction is treated separately under condition (C3), where $A_1 = 0$ and $\rho_3 < 1$.

The chord condition ensures that the motif can consistently replace a straight segment at each refinement step. Iteratively substituting each straight segment with the motif generates the complete self-similar fractal (such as the classical Koch curve). For further background, see Barnsley [44, Chapter II.8], Falconer [45], or Hutchinson [46]. To analyse how a motif is related to the regularity and Lévy areas, we fix a motif given by (3.1). The M segments of the motif define M contractive similarity maps

$$F_k(x) = R(a_k)\, r_k\, x + c_k, \qquad k = 1, \ldots, M,$$

where

- $R(a_k)$ is the rotation matrix, i.e.

$$R(a_k) = \begin{pmatrix} \cos a_k & -\sin a_k \\ \sin a_k & \cos a_k \end{pmatrix},$$

- r_k is the scaling factor (the ratio of contraction),
- c_k is the translation which places the k-th segment at the correct position along the motif. In particular, $c_1 = 0$ and

$$c_k = \sum_{j=1}^{k-1} v_j,\ k = 2, \ldots, M.$$

Starting with the initial segment $S_0 = X_0([0,1])$, where $X_0 : [0,1] \to \mathbb{R}^2$, $X_0(t) = (t, 0)^\top$, and defining the sequence of approximations

$$S_{n+1} = \bigcup_{k=1}^{M} F_k(S_n), \qquad n = 0, 1, 2, \ldots$$

we replace each line segment of S_n by a scaled, rotated, and translated copy of the motif. In this way, we get a sequence $\{S_n : n \in \mathbb{N}\}$. Because every F_k is a contraction (with ratio $r_k < 1$), the family $\{F_k : k = 1, \ldots, M\}$ forms an iterated function system (IFS). By the Banach fixed-point theorem, there exists a unique nonempty compact

set S_∞ satisfying

$$S_\infty = \bigcup_{k=1}^{M} F_k(S_\infty),$$

which is the limiting fractal curve. To use the limiting fractal curve as a driver in a rough differential equation, we require a continuous parametrisation. A natural choice is obtained by using the M-adic expansion of $t \in [0,1]$. Every t has (up to the usual ambiguity on a null set) a base-M expansion

$$t = \sum_{j=1}^{\infty} \frac{i_j - 1}{M^j}, \qquad i_j \in \{1, \dots, M\}.$$

The sequence $I = (i_1, i_2, \dots)$ determines a unique branch of the iterated function system. After n refinement steps, the parameterised point is defined by

$$X_n(t) = F_{i_1} \circ F_{i_2} \circ \cdots \circ F_{i_n}\big(X_0(M^n t - \textstyle\sum_{j=1}^{n}(i_j - 1)M^{n-j})\big), \qquad t \in [0,1],$$

where $X_0(t) = (t, 0)^\top$ is the initial straight segment; the argument of X_0 is the local time in the M-adic interval of generation n containing t. Equivalently, X_n is given by the recursion (3.7) of Section 3.4. Since each F_k is a contraction, the sequence $\{X_n(t)\}_{n\in\mathbb{N}}$ converges uniformly on $[0,1]$ to a continuous limit

$$X(t) = \lim_{n\to\infty} X_n(t),$$

which provides a canonical parametrisation of the fractal curve S_∞. This parametrised limit $X : [0,1] \to \mathbb{R}^2$ is the path that we use as a deterministic control in the rough-path setting. The Hölder exponent α is determined by the scaling of the longest segment:

$$\alpha = \frac{\log(1/r_{\max})}{\log M}, \qquad r_{\max} = \max_k r_k.$$

Because each refinement step replaces every edge by scaled copies of itself plus an intrinsic motif contribution, the Lévy area (and, in general, every signature level) obeys an affine fixed-point equation. Solving that recurrence gives the area of the limiting fractal. Let the motif's partial sums be $w_0 = 0$, $w_j = \sum_{k=1}^{j} v_k$, where v_k is defined in (3.1). The polygon determined by $(w_0, w_1, \dots, w_M)$ has signed area

$$A_1 = \frac{1}{2}\sum_{j=0}^{M-1}\big(w_j \wedge w_{j+1}\big) = \frac{1}{2}\sum_{1\le i<j\le M} v_i \wedge v_j, \tag{3.3}$$

where $x \wedge y := x_1 y_2 - x_2 y_1$ is the two-dimensional wedge product. In terms of (r_k, a_k), we know $v_i \wedge v_j = r_i r_j \sin(a_j - a_i)$, and, hence,

$$A_1 = \frac{1}{2}\sum_{i<j} r_i r_j \sin(a_j - a_i).$$

Let A_n be the Lévy area of the level-n polyline (obtained after n motif replacements). Each edge of level n is replaced by M children that are *similarity transforms* of that edge: *scale by* r_k, *rotate by* a_k, *then translate*. Two facts:

- **Scaling/rotation at level 2:** Lévy area scales like *length*^{2} and is rotation invariant: if X is rotated by R and scaled by r, then $A \mapsto r^2 A$.
- **Chen's identity (concatenation):** The level-2 signature of a concatenation equals the sum of (i) level-2 signatures of the pieces and (ii) the antisymmetric cross contribution coming from the *level-1* increments. For our fixed motif, that cross contribution is exactly the seed A_1 computed above.

With $A_0 = 0$ (straight segment has zero area), A_1 given by (3.3), and

$$\rho = \sum_{k=1}^{M} r_k^2 \in [0, 1), \tag{3.4}$$

the recurrence formula for A_n is given by the following lemma.

Lemma 1. Let A_n be the oriented Lévy area (antisymmetric part of level 2 signature) of the n-th polygonal approximation built from the motif $(v_k = r_k(\cos a_k, \sin a_k))_{k=1}^{M}$, with equal time per piece. Then

$$A_{n+1} \;=\; \rho\, A_n \;+\; A_1 \tag{3.5}$$

where A_1 and ρ are given by (3.3) and (3.4), respectively.

Proof At level $n+1$, the path is the concatenation $\Gamma_{n+1} = \Gamma_n^{(1)} * \cdots * \Gamma_n^{(M)}$ of M *child* copies of the level-n path. The k-th child is an affine image (rotate by a_k, scale by r_k, translate) of Γ_n to fit the k-th motif vector.

For the (antisymmetric) area $A(\cdot)$ we use three facts:

(i) **Area scales quadratically:** under a similarity $x \mapsto R\,(rx)$ (rotation R, factor r), the area multiplies by r^2 and is invariant under R and translation. Hence $A(\Gamma_n^{(k)}) = r_k^2\, A_n$.

(ii) **Chen additivity at level 2:** for a concatenation $\gamma = \gamma^{(1)} * \cdots * \gamma^{(M)}$,

$$S^{(2)}(\gamma) \;=\; \sum_{k=1}^{M} S^{(2)}(\gamma^{(k)}) + \sum_{1 \le i < j \le M} S^{(1)}(\gamma^{(i)}) \otimes S^{(1)}(\gamma^{(j)}).$$

Taking the antisymmetric part (wedge) gives $A(\gamma) = \sum_k A(\gamma^{(k)}) + \frac{1}{2} \sum_{i<j} \big(S^{(1)}(\gamma^{(i)}) \wedge S^{(1)}(\gamma^{(j)})\big)$.

(iii) **Child first levels are motif vectors:** $S^{(1)}(\Gamma_n^{(k)}) = v_k = r_k(\cos a_k, \sin a_k)$ (because the chord of each child equals its motif vector).

Putting these together,

$$A_{n+1} \;=\; \sum_{k=1}^{M} r_k^2 A_n \;+\; \frac{1}{2} \sum_{i<j} v_i \wedge v_j = \Big(\sum_{k=1}^{M} r_k^2\Big) A_n + \frac{1}{2} \sum_{i<j} r_i r_j \sin(a_j - a_i),$$

which is exactly the claimed recurrence with $\rho = \sum r_k^2$ and A_1 as stated. □

We can observe that the recurrence (3.5) has the solution

$$A_n = A_1 \frac{1-\rho^n}{1-\rho}.$$

If $\rho < 1$, the limit Lévy area of the self-similar curve exists and is finite; it is nonzero precisely when $A_1 \neq 0$, and in that case is given by

$$A = \lim_{n\to\infty} A_n = \frac{A_1}{1-\rho}. \tag{3.6}$$

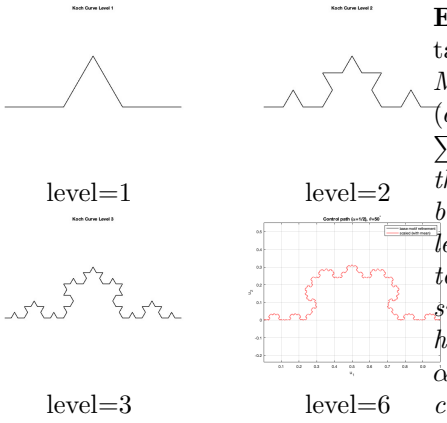


Fig. 1 Koch curves at different iterations: level=1, 2, 3, and 6.

Example 3.1 (classical Koch-type fractal)**.** *The Koch curve is given by* $M = 4$, $r_j = 1/3$, $j = 1,2,3,4$, $(a_1,a_2,a_3,a_4) = (0,\pi/3,-\pi/3,0)$. *Then* $\sum_{k=1}^{4} r_k(\cos a_k, \sin a_k)^\top = (1,0)^\top$, *such that each straight segment is replaced by four segments of one third of its length in the familiar "snowflake" pattern. Here* $A_1 = -\sqrt{3}/36$ *(the triangle of side* $1/3$*, traversed clockwise),* $\rho = 4/9$*, hence* $A = A_1/(1-\rho) = -\sqrt{3}/20$*, and* $\alpha = \log 3/\log 4 \approx 0.79$*. Since* $\alpha > 1/2$*, the classical Koch curve is still in the Young regime; the motifs below are designed to reach* $\alpha = 1/2$ *and* $\alpha = 1/3$*. In Figure 1 we see a classical Koch-type fractal.*

When the objective is to steer the system along a prescribed Lie bracket direction, it is natural to proceed in reverse: given a target Hölder exponent α and a desired Lévy area $\mathbb{A}$, we seek an *algorithm* that constructs a motif (angles a_k and lengths r_k) whose uniform-time self-similar refinement yields a control with the specified regularity and area.

3.2 Designing the control by a Koch-type Fractal

By Corollary 1, to generate a prescribed bracket displacement, one needs to construct a control $\mathbf{X}$ such that the prescribed Hölder exponent α and the target Lévy area $\mathbb{A}_{\text{targ}}$ are achieved. A Koch-type motif can be constructed systematically, and the following procedure provides a reproducible design strategy.

Step (I) **Fixing the Hölder regularity:** We choose an integer $M \geq 3$, the number of segments used to replace each straight piece at each refinement. Under *uniform-time parametrisation* (each subsegment occupies time $1/M$), the Hölder exponent of the limit curve satisfies

$$\alpha \;=\; \frac{\log(1/r_{\max})}{\log M}, \qquad r_{\max} := \max_k r_k.$$

Hence we enforce

$$r_{\max} = M^{-\alpha},$$

which fixes the contraction ratio and guarantees that the limit curve is Hölder continuous with exponent α. In practice, $M = 6$ or $M = 8$ yields simple, visually interpretable motifs and allows for closed-form expressions of the Lévy area.

Step (II) **Fixing a one–parameter "single–bump" motif:** To control the signed area efficiently, we use a one-parameter family of motifs in which the bump angle θ controls the shape and the resulting area. This makes the matching problem $\mathbb{A}(\theta) = \mathbb{A}_{\text{targ}}$ a scalar equation.

Example A (Hölder $\alpha = 1/2$, $M = 6$).

$$(a_1, \ldots, a_6) = (0, 0, +\theta, -\theta, 0, 0), \quad \text{and} \quad (r_1, \ldots, r_6) = (a, a, b, b, a, a),$$

with $b = M^{-1/2} = 6^{-1/2}$ and the unit chord condition

$$4a + 2b\cos\theta = 1 \qquad \Rightarrow \qquad a = \tfrac{1-2b\cos\theta}{4}.$$

From equations (3.4), (3.3), and (3.6), we derive a set of equations for the key quantities. In particular, we find that

$$\rho(\theta) = 4a(\theta)^2 + 2b^2, \quad A_1(\theta) = -\frac{1}{2}b^2\sin(2\theta), \quad \text{and} \quad A(\theta) = \frac{A_1(\theta)}{1-\rho(\theta)}.$$

Since $A_1(\theta) \leq 0$ for $\theta \in (0, \frac{\pi}{2})$, this motif produces negative areas; positive areas are obtained by reflecting the motif ($\theta \mapsto -\theta$). The function $\theta \mapsto A(\theta)$ is *not* monotone on $(0, \frac{\pi}{2})$ (it vanishes at both end points): it decreases strictly on $(0, \theta^*]$, $\theta^* \approx 0.842$ ($\approx 48.2^\circ$), where it attains its minimum $A(\theta^*) \approx -0.1347$, and increases on $[\theta^*, \frac{\pi}{2})$. Hence the equation $A(\theta) = \mathbb{A}_{\text{targ}}$ has a unique solution $\theta \in (0, \theta^*]$ for every $\mathbb{A}_{\text{targ}} \in [-0.1347, 0)$.

Step (III) **Feasibility and Tuning:**

With a single symmetric bump in Example A, the attainable magnitude of A_1 is bounded by

$$|A_1| \leq \frac{1}{2}b^2,$$

and, therefore, we have

$$|\mathbb{A}| \leq \frac{\frac{1}{2}\, b^2}{1-\rho(\theta)}.$$

If the desired area $\mathbb{A}_{\text{targ}}$ lies outside this interval, one can enlarge the admissible range as follows:

- **Reduce ρ:** shorten some flat pieces (smaller r_k), which decreases $\sum r_k^2$ and thus increases $1-\rho$, expanding the range of achievable areas.
- **Add a second bump:** use two pairs of slanted segments $(+\theta_1, -\theta_1)$ and $(+\theta_2, -\theta_2)$. Then $A_1 A_1$ becomes a sum of two sinusoidal contributions in (θ_1, θ_2), giving a wider and more flexible control of A.
- **Change sign:** reversing the bump order or flipping the motif inverts the sign of A.

3.3 Realising a prescribed Lévy area at $\alpha = 1/2$ with a single-bump

We now present a simple one-parameter motif that fixes $\alpha = 1/2$ and realises a prescribed limiting area. Take $M = 6$ and

$$(a_1, \ldots, a_6) = (0,\ 0,\ +\theta,\ -\theta,\ 0,\ 0), \qquad \theta \in (0, \tfrac{\pi}{2}).$$

The third and fourth steps form the "bump" (up and down by $\pm\theta$); the others are flat. We will use two lengths:

$$(r_1, \ldots, r_6) = (a, a, b, b, a, a),$$

with b to fix the Hölder exponent and a adjusted by closure. Next, we fix the exponent. We want $r_{\max} = 6^{-1/2}$ so that

$$\alpha = \frac{\log(1/r_{\max})}{\log 6} = \frac{\log(\sqrt{6})}{\log 6} = \frac{1}{2}.$$

Set $b := 6^{-1/2}$ and ensure $a \leq b$ (which closure will do for us). The horizontal closure condition (3.2) is

$$4a + 2b\cos\theta \ = \ 1 \quad \Longrightarrow \quad a = \frac{1 - 2b\cos\theta}{4}.$$

Since $2b = 2/\sqrt{6} < 1$, we have $a > 0$ for all $\theta \in (0, \frac{\pi}{2})$. Let us now compute ρ and A_1:

$$\begin{aligned} \rho &= \sum_{k=1}^{M} r_k^2 = 4a^2 + 2b^2 \quad \text{and} \\ A_1 &= \frac{1}{2} \sum_{1 \leq i < j \leq M} r_i r_j \sin(a_j - a_i) = -\frac{1}{2}\, b^2 \sin(2\theta). \end{aligned}$$

Observe that the contributions of the pairs formed by one slanted and one flat segment cancel; only the pair $(+\theta, -\theta)$ remains. Finally, we dial the area. As θ varies from 0 to $\pi/4$, A_1 ranges continuously from 0 to $-1/2 b^2$, and returns to 0 as $\theta \to \pi/2$. Since $\rho < 1$ for admissible θ ($0.34 \le \rho \le 0.59$), the limiting area

$$A = \frac{A_1}{1-\rho}$$

takes every value in $[A(\theta^*), 0)$, $A(\theta^*) \approx -0.1347$, exactly once for $\theta \in (0, \theta^*]$, $\theta^* \approx 0.842$; reflecting the motif ($\theta \mapsto -\theta$) gives the positive values. Hence, for every $\mathbb{A}_{\text{targ}} \in (A(\theta^*), 0)$, the equation $A(\theta) = \mathbb{A}_{\text{targ}}$ has exactly two solutions, one in $(0, \theta^*)$ and one in $(\theta^*, \frac{\pi}{2})$, and θ^* itself gives the extremal area $A(\theta^*) \approx -0.1347$. Either branch can be used; restricting to one branch makes the map $\theta \mapsto A(\theta)$ invertible.

3.4 Convergence of the pre-fractals and error bounds

In practice, the limiting fractal driver is not implemented directly; instead one uses the polygonal pre-fractal X_n obtained after n refinement steps. The path X_n is piecewise linear with M^n pieces, and its derivative is therefore a piecewise constant control. In this subsection we show that the rough path lifts of the pre-fractals converge geometrically in n, with a rate that is explicit in the motif, and we translate this into an explicit bound on the steering error over a window of length τ.

Setting. We fix a motif $(r_k, a_k)_{k=1}^M$ satisfying the chord condition (3.2), and write $F_k(x) = c_k + r_k R(a_k)x$ with $c_1 = 0$ and $c_k = \sum_{j<k} v_j$. With uniform time, the k-th motif segment occupies $I_k = [\frac{k-1}{M}, \frac{k}{M}]$. The pre-fractals are defined recursively by $X_0(t) = t\, e_1$ and

$$X_{n+1}(t) = F_k\big(X_n(Mt - k + 1)\big), \qquad t \in I_k,\ k = 1, \dots, M. \tag{3.7}$$

X_n is piecewise linear with M^n pieces, and all its vertices lie on the fractal. For a word $w = (w_1, \dots, w_j)$ let I_w be the M-adic interval of generation j (length M^{-j}), $F_w = F_{w_1} \circ \cdots \circ F_{w_j}$ and $r_w = r_{w_1} \cdots r_{w_j}$. Iterating (3.7) gives, for $j \le n$,

$$X_n\big|_{I_w} = F_w \circ X_{n-j} \circ \phi_w, \tag{3.8}$$

where $\phi_w : I_w \to [0,1]$ is the increasing affine bijection. We set

$$r_{\max} = \max_k r_k = M^{-\alpha}, \qquad \rho_q := \sum_{k=1}^{M} r_k^q \quad (q = 2, 3),$$

so that $\rho_2 = \rho$ from (3.4).

We denote by $\mathbf{X}_n = (X_n^{(1)}, \dots, X_n^{(N)})$ the canonical lift of X_n (iterated Riemann–Stieltjes integrals) truncated at level N. We equip $(\mathbb{R}^2)^{\otimes k}$ with the Euclidean (Hilbert–Schmidt) norm $|\cdot|$, for which $R^{\otimes k}$ is an isometry for every rotation R. For $\beta \in (0, 1]$

we use the inhomogeneous β-Hölder rough path norm and distance

$$\|\mathbf{X}\|_\beta = \sum_{k=1}^{N} \sup_{s<t} \frac{|X^{(k)}_{s,t}|}{|t-s|^{k\beta}}, \qquad d_\beta(\mathbf{X},\mathbf{Y}) = \sum_{k=1}^{N} \sup_{s<t} \frac{|X^{(k)}_{s,t} - Y^{(k)}_{s,t}|}{|t-s|^{k\beta}}.$$

Two algebraic facts. (i) If $F(x) = c + rRx$ is a similarity, then the signature of $F \circ \gamma$ is obtained from that of γ by

$$S^{(k)}(F \circ \gamma) = r^k R^{\otimes k} S^{(k)}(\gamma).$$

In particular, the Lévy area is multiplied by r^2, since antisymmetric 2-tensors in $\mathbb{R}^2$ are multiples of $e_1 \otimes e_2 - e_2 \otimes e_1$ and $\det R = 1$. (ii) Signatures are invariant under reparametrisation of time. Together with Chen's identity, applied to the M pieces in (3.7), this gives

$$S(X_{n+1})_{0,1} = \bigotimes_{k=1}^{M} \delta_{r_k} R_k \, S(X_n)_{0,1}, \tag{3.9}$$

where δ_r multiplies level k by r^k and R_k acts as $R(a_k)^{\otimes k}$ on level k. Let us analyse the change in the signature over the full interval $[0,1]$ between two successive refinement levels.

Lemma 2. Let $D^{(k)}_n := X^{(k)}_{n+1;0,1} - X^{(k)}_{n;0,1}$. Then:

1. $D^{(1)}_n = 0$ for all n.
2. The symmetric part of $D^{(2)}_n$ vanishes, and its antisymmetric part is equal to $(A_{n+1} - A_n)(e_1 \otimes e_2 - e_2 \otimes e_1)$ with $A_{n+1} - A_n = \rho_2^n A_1$. In particular $|D^{(2)}_n| = \sqrt{2}\,\rho_2^n |A_1|$.
3. If $A_1 = 0$, then $D^{(3)}_n = T_3^n D^{(3)}_0$ with $T_3 = \sum_k r_k^3 R(a_k)^{\otimes 3}$. Hence $|D^{(3)}_n| \le \rho_3^n |D^{(3)}_0|$.

Proof (1) The assertion follows since all X_n run from 0 to e_1. (2) Since all paths X_n have the same increment e_1, the shuffle identity gives $\operatorname{Sym} X^{(2)}_{n;0,1} = \frac{1}{2}\, e_1 \otimes e_1$, for every n. Hence,

$$\operatorname{Sym} D^{(2)}_n = \operatorname{Sym}\big(X^{(2)}_{n+1;0,1} - X^{(2)}_{n;0,1}\big) = 0.$$

It remains to consider the antisymmetric part. In dimension two every antisymmetric 2-tensor is a scalar multiple of $E := e_1 \otimes e_2 - e_2 \otimes e_1$. Moreover, for every rotation $R \in SO(2)$, $R^{\otimes 2} E = (Re_1) \otimes (Re_2) - (Re_2) \otimes (Re_1) = (\det R)\, E = E$. Thus rotations leave the antisymmetric direction E invariant. From the level-2 recursion, we obtain

$$D^{(2)}_n = \sum_k r_k^2 R_k^{\otimes 2} D^{(2)}_{n-1}.$$

Since $D^{(2)}_{n-1}$ is antisymmetric, we may write $D^{(2)}_{n-1} = c_{n-1} E$ for some scalar c_{n-1}. Therefore

$$D^{(2)}_n = \sum_k r_k^2 c_{n-1} R_k^{\otimes 2} E = \left(\sum_k r_k^2\right) c_{n-1} E = \rho_2\, c_{n-1} E.$$

Consequently,

$$c_n = \rho_2 c_{n-1}.$$

Since $c_0 = A_1 - A_0 = A_1$, we obtain

$$c_n = \rho_2^n A_1.$$

Equivalently,

$$D_n^{(2)} = (A_{n+1} - A_n)(e_1 \otimes e_2 - e_2 \otimes e_1), \qquad A_{n+1} - A_n = \rho_2^n A_1.$$

Finally, since

$$|e_1 \otimes e_2 - e_2 \otimes e_1| = \sqrt{2},$$

we obtain

$$|D_n^{(2)}| = \sqrt{2}\,\rho_2^n |A_1|.$$

This is consistent with Lemma 1.

(3) If $A_1 = 0$, then $A_n = 0$ for all n, so the level 1 and level 2 data of every piece in (3.9) are independent of n. Consequently, all level 3 terms in (3.9) involving only levels 1 and 2 cancel when consecutive refinement levels are subtracted, and

$$D_n^{(3)} = T_3 D_{n-1}^{(3)}.$$

Iterating this identity gives

$$D_n^{(3)} = T_3^n D_0^{(3)}.$$

Since every $R(a_k)^{\otimes 3}$ is an isometry for the Hilbert–Schmidt norm,

$$\|T_3\| \le \sum_k r_k^3 \|R(a_k)^{\otimes 3}\| = \sum_k r_k^3 = \rho_3.$$

Hence

$$|D_n^{(3)}| \le \rho_3^n |D_0^{(3)}|.$$

□

Lemma 2 measures the refinement on the full interval. The next lemma shows where it happens: the step $n \to n+1$ leaves all vertices of generation n fixed and adds M^n disjoint micro-bumps, one in every M-adic interval of generation n.

Lemma 3. Let $n \ge 0$ and let w be a word of length n. Then:

1. $X_{n+1}(t) = X_n(t)$ for every $t \in M^{-n}\mathbb{Z} \cap [0,1]$.
2. On I_w we have $X_n = F_w \circ X_0 \circ \phi_w$ (a straight segment) and $X_{n+1} = F_w \circ X_1 \circ \phi_w$ (a copy of the motif, scaled by r_w). Consequently

$$\sup_{t \in I_w} |X_{n+1}(t) - X_n(t)| = r_w \, \|X_1 - X_0\|_\infty \le M^{-n\alpha} \, \|X_1 - X_0\|_\infty.$$

3. The increments of X_{n+1} and X_n over I_w coincide, and their Lévy areas over I_w differ by

$$\mathbb{A}(X_{n+1})(I_w) - \mathbb{A}(X_n)(I_w) = r_w^2 A_1, \qquad |r_w^2 A_1| \le M^{-2n\alpha} |A_1|.$$

4. Summing (3) over all words of length n gives back Lemma 2(2): $D_n^{(2)} = \big(\sum_{|w|=n} r_w^2\big) A_1 E = \rho_2^n A_1 E$.

Proof (1) and (2): By (3.8) with $j = n$, applied to X_n and to X_{n+1}, we get $X_n|_{I_w} = F_w \circ X_0 \circ \phi_w$ and $X_{n+1}|_{I_w} = F_w \circ X_1 \circ \phi_w$. Since X_0 and X_1 both run from 0 to e_1, the two paths agree at the end points of I_w, which proves (1). F_w is a similarity with ratio $r_w \le r_{\max}^n = M^{-n\alpha}$, which proves (2). (3): The increments agree by (1). By fact (i), the area of $F_w \circ \gamma$ is r_w^2 times the area of γ. The segment X_0 has area 0 and the motif polygon X_1 has area A_1. (4): By Chen's identity over the M^n intervals I_w, the level-2 signature on $[0,1]$ is the sum of the level-2 signatures of the pieces plus cross terms. The cross terms involve only the level-1 increments of the pieces, so by (1) they are the same for X_n and X_{n+1} and cancel in $D_n^{(2)}$. The symmetric parts cancel for the same reason. Finally, $\sum_{|w|=n} r_w^2 = (\sum_k r_k^2)^n = \rho_2^n$. □

Remark 1. Lemma 3 makes precise in what sense the pre-fractals become *finer*. Going from level n to level $n+1$ does not move the M^n+1 grid points. It only inserts M^n micro-bumps, each of diameter at most $M^{-n\alpha}\|X_1 - X_0\|_\infty$ and signed area $r_w^2 A_1$. For $\alpha = 1/2$ these are of order $M^{-n/2}$ and $M^{-n}|A_1|$. The total added area $\rho_2^n A_1$ is a sum of M^n contributions, each of size $O(M^{-2n\alpha})$.

We can now formulate a convergence result for the pre-fractals.

Theorem 1. Let $\alpha \in (\frac{1}{4}, \frac{1}{2}]$, $r_{\max} = M^{-\alpha}$, and let $\beta < \alpha$ be such that $N := \lfloor 1/\beta \rfloor$ satisfies $N = 2$ if $\alpha > \frac{1}{3}$ and $N = 3$ if $\alpha \le \frac{1}{3}$. Assume

(C2) if $N = 2$: $\rho_2 < 1$;
(C3) if $N = 3$: $A_1 = 0$ and $\rho_3 < 1$.

Set

$$\lambda := \max\left\{\rho_N,\ M^{-(\alpha-\beta)}\right\} < 1.$$

Then there are constants K, C, depending on the motif, β and N but *not* on n, such that:

(a) $\sup_n \|\mathbf{X}_n\|_\alpha \le K$;
(b) $d_\beta(\mathbf{X}_n, \mathbf{X}_{n+1}) \le C\lambda^n$. Consequently $(\mathbf{X}_n)$ converges to a geometric β-Hölder rough path $\mathbf{X}$ whose first level is the fractal X, and

$$d_\beta(\mathbf{X}_n, \mathbf{X}) \le \frac{C}{1-\lambda}\,\lambda^n; \tag{3.10}$$

(c) on the full interval the errors are explicit: if $N = 2$, $\mathbb{A}(\mathbf{X})_{0,1} - \mathbb{A}(\mathbf{X}_n)_{0,1} = \rho_2^n A$ with $A = A_1/(1-\rho_2)$ as in (3.6); if $N = 3$, $|X^{(3)}_{0,1} - X^{(3)}_{n;0,1}| \le \rho_3^n |D_0^{(3)}|/(1-\rho_3)$.

Proof The proof consists of four steps. We first derive the estimates on (M)-adic intervals, separately for scales above and below the refinement level. We then extend these estimates to arbitrary intervals using the Chen identity and, in the final step, pass to the limit in the rough path metric.

Step (i) *M-adic intervals of generation $j \le n$.* By (3.8) and fact (i), $X_n^{(k)}(I_w) = r_w^k R_w^{\otimes k} X^{(k)}_{n-j;0,1}$, where R_w is the product of the rotations along w. Since $r_w \le M^{-j\alpha} = |I_w|^\alpha$

and $\sup_m |X^{(k)}_{m;0,1}| < \infty$ by Lemma 2, we get $|X^{(k)}_n(I_w)| \le K_0 |I_w|^{k\alpha}$. For the differences, we obtain

$$\frac{|X^{(k)}_{n+1}(I_w) - X^{(k)}_n(I_w)|}{|I_w|^{k\beta}} \le M^{-jk(\alpha-\beta)}\, |D^{(k)}_{n-j}| \le c\, M^{-jk(\alpha-\beta)} \rho_N^{n-j} \le c\, \lambda^n.$$

Step (ii) *generation $j > n$.* On I_w, the path X_n is a piece of a single segment of length $r_{w|n} \le M^{-n\alpha}$ traversed in time M^{-n}. Hence $|X_n(I_w)| \le M^{-n\alpha} M^{n-j} \le |I_w|^\alpha$, and $|X^{(k)}_n(I_w)| = |X_n(I_w)|^k/k! \le |I_w|^{k\alpha}$. The same holds for X_{n+1} if $j > n+1$, and by Step 1 if $j = n+1$. Consequently, the difference divided by $|I_w|^{k\beta}$ is at most $2|I_w|^{k(\alpha-\beta)} \le 2M^{-nk(\alpha-\beta)} \le 2\lambda^n$.

Step (iii) *Arbitrary intervals.* If $M^{-j_0-1} < t - s \le M^{-j_0}$, then $[s,t]$ is the concatenation of at most $2(M-1)$ M-adic intervals of each generation $j \ge j_0 + 1$. By Chen's identity, $\mathbf{X}_{n;s,t}$ is the ordered product of their signatures. The bounds of Steps 1–2 on these intervals, with exponent α for the norms and β for the differences, sum geometrically over j. This yields (a) and (b) with constants independent of n (cf. the proof of the Kolmogorov criterion for rough paths in [10, Ch. 3]).

Step (iv) *The limit.* By (b), $(\mathbf{X}_n)$ is Cauchy for d_β. The β-Hölder rough paths form a complete metric space, and limits of canonical lifts of piecewise linear paths are geometric by definition. The first level converges uniformly to the fractal parametrisation, and (3.10) follows by summing the geometric series. Part (c) follows from Lemma 2 by summation, e.g.

$$A - A_n = \sum_{m \ge n} \rho_2^m A_1 = \frac{\rho_2^n A_1}{1 - \rho_2} = \rho_2^n A;$$

similarly, $|X^{(3)}_{0,1} - X^{(3)}_{n;0,1}| \le \sum_{m \ge n} \rho_3^m |D^{(3)}_0| = \rho_3^n |D^{(3)}_0|/(1-\rho_3)$.

□

Remark 2. Let us briefly explain why $\rho_N < 1$ is essential. Since $r_{\max} = M^{-\alpha}$, we have $\rho_{1/\alpha} = \sum_k r_k^{1/\alpha} \le M\, r_{\max}^{1/\alpha} = 1$, with equality iff all r_k are equal. At $\alpha = 1/2$ with equal lengths, Lemma 1 gives $A_n = nA_1$, so the areas of the polygonal approximations diverge whenever $A_1 \ne 0$. Thus, for the present self-similar construction with equal segment lengths and $A_1 \ne 0$, the Lévy areas diverge linearly at Hölder regularity $1/2$. Condition (C2) excludes it: the motif must contain segments of different lengths. The same mechanism at level 3 explains (C3).

From rough path distance to steering error. Over the design window $[0,\tau]$ we use a closed loop. Let Y be X traversed on $[0, 1/2]$, followed by the straight return from e_1 to 0 on $[1/2, 1]$, and define Y_n from X_n in the same way. The return segment has zero area and zero cross term with X (since $e_1 \wedge (-e_1) = 0$). By Chen's identity, we obtain, therefore, $Y^{(1)}_{0,1} = 0$, $\mathbb{A}(Y)_{0,1} = \mathbb{A}(X)_{0,1}$, and all full-interval differences in Theorem 1(c) are the same for Y_n as for X_n. (If $A_1 = 0$, a direct computation gives $Y^{(3)}_{0,1} = X^{(3)}_{0,1} - 1/6 e_1^{\otimes 3}$.) Moreover $d_\beta(\mathbf{Y}_n, \mathbf{Y}) \le C\, d_\beta(\mathbf{X}_n, \mathbf{X})$. We compress the loop into the window,

$$Y^\tau_t := \tau^\alpha\, Y_{t/\tau}, \qquad t \in [0,\tau],$$

so that level k of the full-window signature is $\tau^{k\alpha}$ times that of Y. We compare the solution $x^{(n)}$ of the ODE driven by the piecewise linear path Y^τ_n (equivalently, by its piecewise constant derivative control) with the solution x of the RDE driven by $\mathbf{Y}^\tau$.

The next Corollary gives the explicit steering error.

Corollary 2. Let the assumptions of Theorem 1 hold, let $V_1, V_2 \in C_b^\gamma$ with $\gamma > 1/\beta$, and let $\tau \in (0,1]$. Then, with constants C_1, C_2, L depending on V and the motif but not on n or τ:

(i) (rough path distance) $|x_\tau^{(n)} - x_\tau| \le C_1\, \tau^\alpha \lambda^n$;
(ii) ($N = 2$, second-order brackets)

$$\left| x_\tau^{(n)} - x_0 - \tau^{2\alpha} A\,[V_1, V_2](x_0) \right| \le L\, \tau^{2\alpha} \rho_2^n |A| + C_2\, \tau^{3\alpha};$$

(iii) ($N = 3$, third-order brackets)

$$\left| x_\tau^{(n)} - x_0 - \tau^{3\alpha} \big(\ell^{1,(1,2)} [V_1,[V_1,V_2]] + \ell^{2,(1,2)} [V_2,[V_1,V_2]] \big)(x_0) \right| \le L\, \tau^{3\alpha} \rho_3^n |D_0^{(3)}| / 1 - \rho_3 + C_2\, \tau^{4\alpha},$$

with $\ell^{1,(1,2)} = Y_{0,1}^{112}$ and $\ell^{2,(1,2)} = -Y_{0,1}^{122}$.

For $\alpha = 1/2$ in (ii) and $\alpha = 1/3$ in (iii), the main term is of order τ, and the errors are $O(\tau \rho_N^n) + O(\tau^{3/2})$ and $O(\tau \rho_3^n) + O(\tau^{4/3})$, respectively.

Proof (i) By scaling, we know

$$d_{\beta;[0,\tau]}(\mathbf{Y}_n^\tau, \mathbf{Y}^\tau) = \sum_k \tau^{k(\alpha-\beta)} \sup \frac{|\Delta Y_{s,t}^{(k)}|}{|t-s|^{k\beta}} \le \tau^{\alpha-\beta} d_\beta(\mathbf{Y}_n, \mathbf{Y}).$$

Likewise all β-Hölder norms on $[0,\tau]$ are bounded by K, uniformly in n and $\tau \le 1$. The local Lipschitz continuity of the Itô–Lyons map [9, 10] gives $\|x^{(n)} - x\|_{\beta;[0,\tau]} \le C\, d_{\beta;[0,\tau]}(\mathbf{Y}_n^\tau, \mathbf{Y}^\tau)$. Since $x_0^{(n)} = x_0$, we have $|x_\tau^{(n)} - x_\tau| \le \tau^\beta \|x^{(n)} - x\|_{\beta;[0,\tau]}$, and (3.10) completes the proof.

(ii) The step-N log-ODE estimate [9, Ch. 10] with $\omega(s,t) = (\tau^\alpha K)^{1/\beta}(t-s)/\tau$ gives $|x_\tau^{(n)} - z_1^{(n)}| \le C(\tau^\alpha K)^{N+1}$, where $z^{(n)}$ solves (1.12) with the log-signature of $\mathbf{Y}_n^\tau$. For $N = 2$ this log-signature is $\tau^{2\alpha} A_n [e_1, e_2]$ with $A_n = (1 - \rho_2^n) A$, so $z_1^{(n)}$ is the time-one flow of $\tau^{2\alpha} A_n [V_1, V_2]$. By Grönwall's inequality, $|z_1^{(n)} - z_1| \le L\tau^{2\alpha} |A - A_n| = L\tau^{2\alpha} \rho_2^n |A|$. Finally, $z_1 = x_0 + \tau^{2\alpha} A[V_1, V_2](x_0) + O(\tau^{4\alpha})$, and $4\alpha \ge 3\alpha$.

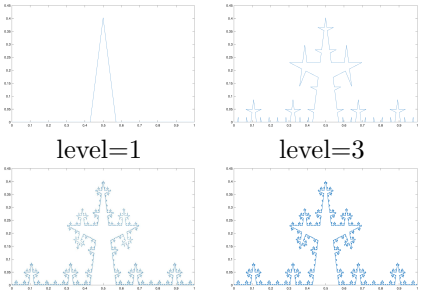
(iii) The proof is the same. Levels 1 and 2 of $\mathbf{Y}_n^\tau$ vanish on $[0,\tau]$, so the log-signature is the Lie element $\tau^{3\alpha} Y_{n;0,1}^{(3)}$, whose coordinates are given in (1.8). □

Remark 3. For $\alpha = 1/2$, Corollary 2(ii) gives the relative error of the bracket displacement:

$$\frac{\left| x_\tau^{(n)} - x_0 - \tau A[V_1, V_2](x_0) \right|}{\tau |A|\, |[V_1, V_2](x_0)|} \;\lesssim\; \rho_2^n + \tau^{1/2}.$$

A tolerance ε is therefore met with $n \ge \log \varepsilon / \log \rho_2$ refinement steps and a window $\tau \lesssim \varepsilon^2$. For the single-bump motif of Example A with $\theta = \pi/4$ one has $\rho_2 \approx 0.378$, so $n = 5$ already gives a bias below 1%. Two further observations are useful in practice:

- Since $A_n = A_1(1-\rho_2^n)/(1-\rho_2)$ is explicit, the bias can be removed altogether by choosing θ so that $A_n(\theta) = A_{\mathrm{targ}}$ for the chosen n. Only the $O(\tau^{3\alpha})$ term then remains, with a constant that does not depend on n.
- Refinement has a price. The largest input amplitude of Y_n^τ is of order $\tau^{\alpha-1}(Mr_{\max})^n = \tau^{\alpha-1}M^{n(1-\alpha)}$, which grows geometrically in n. The choice of n is a trade-off between the area bias ρ_2^n and actuator amplitude. Theorem 1 guarantees that this trade-off can be made without any deterioration of the constants.



Example 3.2 (A generalised Koch-type fractal)**.** *The motif is given by* $M = 6$, $a = 0.2146$, $b = 0.4082$, $\theta = \pi/2.25$ *(*$= 80°$*),* $(r_1, r_2, \dots, r_6) = (a, a, b, b, a, a)$, $(a_1, \dots, a_6) = (0, 0, \theta, -\theta, 0, 0)$. *From the formulas of Example A we get* $A_1 = -1/2 b^2 \sin(2\theta) = -0.0285$, $\rho = 4a^2 + 2b^2 = 0.5175$ *and* $A = A_1/(1-\rho) = -0.0591$. *Since* $\theta \mapsto A(\theta)$ *is strictly decreasing on* $(0, \theta^*]$ *and strictly increasing on* $[\theta^*, \pi/2)$, $\theta^* \approx 0.842$, *it is invertible on each of the two branches; here* θ *lies on the second one. The same area is also obtained on the first branch, with the flatter bump* $\theta \approx 0.242$ *(*$\approx 13.9°$*). In the Figure on the left we see the generalised Koch-type fractal.*

Corollary 2 controls the end point x_τ. We now control the whole trajectory on $[0, \tau]$ and consider two refinements of the input: (a) increasing the level n; (b) repeating the loop K times inside the window. In what follows, $\Phi_{s,t}^{\mathbf{Z}}$ denotes the solution flow of the equation driven by $\mathbf{Z}$ from time s to time t.

Proposition 2. Let the assumptions of Corollary 2 hold with $N = 2$, and assume in addition $V_1, V_2 \in C_b^{\gamma+1}$. Let $x^{(n)}$ be the solution driven by Y_n^τ. There are constants L, C, independent of n and $\tau \in (0, 1]$, such that:

(i) at the grid times $t \in \tau\, \frac{1}{2} M^{-n}\mathbb{Z} \cap [0, \tau]$,

$$|x_t^{(n+1)} - x_t^{(n)}| \le L\Big(\tau^{2\alpha}\rho_2^n |A_1|\, \|[V_1, V_2]\|_\infty + C\,\tau^{3\alpha}\rho_3^n\Big);$$

(ii) for all $t \in [0, \tau]$,

$$|x_t^{(n+1)} - x_t^{(n)}| \le L\Big(\tau^{2\alpha}\rho_2^n |A_1|\, \|[V_1, V_2]\|_\infty + C\,\tau^{3\alpha}\rho_3^n + C\,\tau^{\alpha} M^{-n\alpha}\Big);$$

(iii) $x^{(n)} \to x$ uniformly on $[0, \tau]$, and $\sup_{t \le \tau} |x_t^{(n)} - x_t| \le C\big(\tau^{2\alpha}\rho_2^n + \tau^\alpha M^{-n\alpha}\big)$.

Proof Let $J_1, \dots, J_{M^n}$ be the images in $[0, \tau/2]$ of the M-adic intervals of generation n. On the return segment the drivers Y^τ_{n+1} and Y^τ_n coincide.

Local comparison. Fix $J = J_i$ with word w and a point y. By Lemma 3, the two drivers have the same increment h on J, and their areas differ by $\tau^{2\alpha} r_w^2 A_1$. Both drivers have 1-variation at most $c\,\tau^\alpha r_w$ on J, with $c = \sum_k r_k$. The step-2 log-ODE estimate (Proposition 1) applies to each driver. The two resulting log-ODE flows have the same drift $h \cdot V$ and differ only in the coefficient of $[V_1, V_2]$. By Grönwall's inequality,

$$\left|\Phi^{n+1}_J(y) - \Phi^n_J(y)\right| \le e^C\, \tau^{2\alpha} r_w^2 |A_1|\, \|[V_1, V_2]\|_\infty + C\, \tau^{3\alpha} r_w^3.$$

Propagation (telescoping over the J_i). Write t_i for the right end point of J_i and $y_i := x^{(n+1)}_{t_{i-1}}$. Then

$$x^{(n+1)}_{t_m} - x^{(n)}_{t_m} = \sum_{i \le m} \Big(\Phi^n_{t_i, t_m}\big(\Phi^{n+1}_{J_i}(y_i)\big) - \Phi^n_{t_i, t_m}\big(\Phi^n_{J_i}(y_i)\big) \Big).$$

The flows $\Phi^n_{s,t}$ are Lipschitz in the initial point. The Lipschitz constant L depends only on $\|V\|_{C_b^{\gamma+1}}$ and on a bound for the rough path norm of the driver [9, Ch. 11]. By Theorem 1(a) that norm is bounded uniformly in n and $\tau \le 1$. Summing the local bound and using $\sum_{|w|=n} r_w^q = \rho_q^n$ gives (i).

For (ii), let $t \in J_m$. Apply (i) at t_{m-1} and compare the two flows on $[t_{m-1}, t]$. Here the level-1 increments may differ, by at most $\tau^\alpha r_w \|X_1 - X_0\|_\infty \le \tau^\alpha M^{-n\alpha} \|X_1 - X_0\|_\infty$ (Lemma 3(2)). The local Lipschitz continuity of the Itô–Lyons map on J_m then gives the additional term.

(iii) By Corollary 2(i) and the proof given there, $x^{(n)} \to x$ uniformly. Sum (ii) over $m \ge n$, using $\rho_3 \le r_{\max}\rho_2 < \rho_2$. □

Remark 4. Proposition 2 is the trajectory-level counterpart of Lemma 3. Passing from level n to level $n+1$ changes the motion in two ways. First, it adds small wiggles of amplitude $O(\tau^\alpha M^{-n\alpha})$ inside each grid interval. Second, it adds a transverse drift in the bracket direction, of total size $O(\tau^{2\alpha}\rho_2^n)$, built from M^n micro bracket steps. The micro step on J_w has size $\tau^{2\alpha} r_w^2 |A_1|$, which is $O(\tau M^{-n})$ for $\alpha = 1/2$. Both corrections tend to 0 geometrically, so the motion becomes *finer and finer*. However, the envelope of the motion does not shrink with n. The excursion along the first driving direction stays of order $\tau^\alpha \sup_t |Y^1_t|$ for every n. To make the envelope small one has to repeat the loop, as follows.

In the next proposition we study what happens when both the number of repetitions K and the refinement level n are increased. In practice, the loop is executed K times within the same time window $[0, \tau]$, each time on a window of length τ/K and with amplitude $(\tau/K)^{1/2}$. Each loop moves the system by approximately $\frac{\tau}{K} A_n[V_1, V_2]$, so after K loops the total displacement in the Lie bracket direction is still $\tau A_n[V_1, V_2]$, independently of K. What changes with K is the path taken to get there. The oscillations generated by a single loop have size of order $(\tau/K)^{1/2}$, so they become narrower as K grows. The trajectory therefore stays in an ever thinner tube around the integral curve of the bracket field. For the unicycle this curve is a straight segment perpendicular to the initial heading. Hence the motion of the unicycle converges to a straight sideways motion, and its back-and-forth oscillations become narrower and narrower. The two parameters play different roles:

- increasing K makes the motion narrower: the width of the tube decreases like $K^{-1/2}$, and the end point error due to the log-ODE remainder decreases like $\tau^{3/2}K^{-1/2}$;
- increasing n makes the motion more accurate: the area bias $|A - A_n| = \rho_2^n|A|$ tends to zero, so the length of the segment tends to the prescribed value $\tau|A|$.

For $K \in \mathbb{N}$, let $U^{n,K}$ be the concatenation of K copies of the loop, each compressed to a window of length τ/K:

$$U_t^{n,K} := \Big(\frac{\tau}{K}\Big)^{\alpha} Y_n\Big(\frac{Kt}{\tau} - i\Big), \qquad t \in \Big[\frac{i\tau}{K}, \frac{(i+1)\tau}{K}\Big],\ i = 0, \dots, K-1,$$

and let $x^{(n,K)}$ be the corresponding solution. Since each loop is closed, $U^{n,K}$ is continuous.

Proposition 3. Let $\alpha = 1/2$ and let the assumptions of Corollary 2(ii) hold. Let $z_t^{(n)} := \exp\big(t\, A_n[V_1, V_2]\big)(x_0)$ be the integral curve of the bracket field $A_n[V_1, V_2]$, and let z_t be the same curve with A in place of A_n. There are constants C, L, independent of n, K and $\tau \in (0, 1]$, such that:

(i) at the loop end points $t = i\tau/K$, $|x_t^{(n,K)} - z_t^{(n)}| \le C\,\tau^{3/2}K^{-1/2}$;
(ii) for all $t \in [0, \tau]$, $|x_t^{(n,K)} - z_t^{(n)}| \le C\,(\tau/K)^{1/2}$;
(iii) $|x_\tau^{(n,K)} - z_\tau| \le L\,\tau\,\rho_2^n|A| + C\,\tau^{3/2}K^{-1/2}$.

In particular, the trajectory converges uniformly to the curve z as $n, K \to \infty$.

Proof (i) By Corollary 2(ii), with window τ/K, one loop maps y to $\exp\big(\frac{\tau}{K}A_n[V_1, V_2]\big)(y) + O\big((\tau/K)^{3/2}\big)$. The constant is uniform in n by Theorem 1(a), and uniform in y. The flow of the smooth field $A_n[V_1, V_2]$ is Lipschitz with constant $e^{L\tau}$ on $[0, \tau]$. Telescoping over the $i \le K$ loops, exactly as in the proof of Proposition 2, gives the error $K \cdot C(\tau/K)^{3/2} = C\tau^{3/2}K^{-1/2}$. (ii) Inside one loop, the solution moves by at most $C\|U^{n,K}\|_{\alpha;[i\tau/K,(i+1)\tau/K]}(\tau/K)^{1/2} \le C(\tau/K)^{1/2}$. Here we use the uniform bound of Theorem 1(a) and scaling. On the same interval, $z^{(n)}$ moves by $O(\tau/K)$. (iii) Combine (i) with $|z_\tau^{(n)} - z_\tau| \le L\tau|A - A_n| = L\tau\rho_2^n|A|$ (Grönwall and Theorem 1(c)). □

The unicycle driven by a Koch-type loop

We now work out Example 2.1 with the drivers of this section. As in Section 3.4, let Y be the loop obtained by traversing the fractal X of a motif on $[0, \frac{1}{2}]$ and returning along the chord from e_1 to 0 on $[\frac{1}{2}, 1]$; Y_n is defined in the same way from the pre-fractal X_n. The return segment adds neither area nor a cross term, so $Y_{0,1} = 0$ and $\mathbb{A}(Y)_{0,1} = A = A_1/(1-\rho)$, $\mathbb{A}(Y_n)_{0,1} = A_n = A_1(1-\rho^n)/(1-\rho)$. On a window $[0, \tau]$ we use the driving path

$$U_t = \tau^{1/2}\, Y_{t/\tau}, \qquad t \in [0, \tau],$$

i.e. the forward speed is $u_1 = \dot{U}^1$ (first coordinate of the loop) and the turn rate is $u_2 = \dot{U}^2$ (second coordinate). For the pre-fractal Y_n both inputs are piecewise constant.

Example 3.3. (Log-ODE for the unicycle.)

For the unicycle, the step-2 log-ODE (2.4) on a window $[s,t]$ can be solved in closed form. Write $c := X^2_{s,t}$ (net turning), $X^1_{s,t}$ (net forward motion) and $\mathbb{A} = \mathbb{A}^{12}_{s,t}$. With $[V_1,V_2](x) = (\sin x_3, -\cos x_3, 0)^\top$ from (2.2), the auxiliary ODE reads (compare (1.12))

$$\dot z_\rho = X^1_{s,t}\begin{pmatrix}\cos z_3\\ \sin z_3\\ 0\end{pmatrix} + c\begin{pmatrix}0\\0\\1\end{pmatrix} + \mathbb{A}\begin{pmatrix}\sin z_3\\ -\cos z_3\\ 0\end{pmatrix}, \qquad z_0 = x_s,$$

so $z_3(\rho) = \theta_s + c\rho$, and integrating over $\rho\in[0,1]$ gives

$$\begin{aligned} x_1(t) - x_1(s) &\approx X^1_{s,t}\,\frac{\sin(\theta_s+c)-\sin\theta_s}{c} + \mathbb{A}\,\frac{\cos\theta_s-\cos(\theta_s+c)}{c},\\ x_2(t) - x_2(s) &\approx X^1_{s,t}\,\frac{\cos\theta_s-\cos(\theta_s+c)}{c} - \mathbb{A}\,\frac{\sin(\theta_s+c)-\sin\theta_s}{c},\\ \theta(t)-\theta(s) &= c, \end{aligned}$$

(with the limits $c\to 0$ understood), with an error $O(\omega(s,t)^{3/p})$ by Proposition 1. For the loop U on $[0,\tau]$ we have $X^1_{0,\tau} = c = 0$ and $\mathbb{A} = \tau A$, hence

$$x_\tau - x_0 = \tau A\,\big(\sin\theta_0,\,-\cos\theta_0,\,0\big)^\top + O(\tau^{3/2}),$$

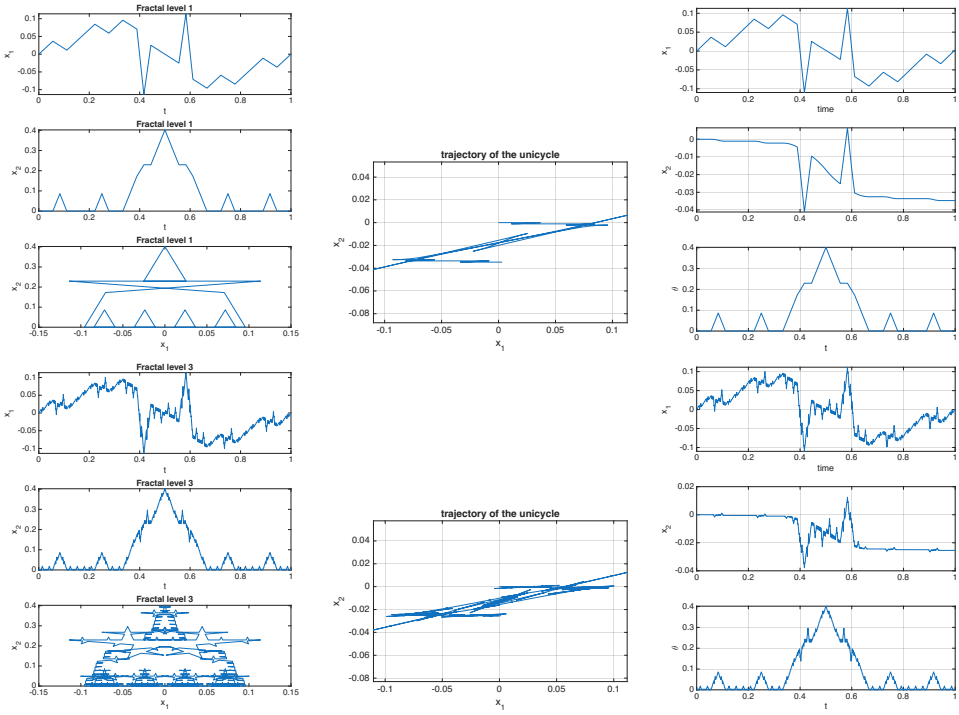
a pure sideways motion perpendicular to the initial heading, of size $|A|\tau$.

Example 3.4. Numerical simulation. *We take the motif of Example A with $\theta = \pi/2.25$, i.e. $b = 6^{-1/2}$ and $a = (1-2b\cos\theta)/4 = 0.2146$. It follows that $\rho = 0.517467 < 1$ and the Lévy area $A_1 = -0.028502$, so $A_n = A_1(1-\rho^n)/(1-\rho)$ and $A = -0.0591$. In contrast to the construction above, the loop in this simulation is closed by subtracting the drift, $Y_n(t) = X_n(t) - t\,e_1$, $t\in[0,1]$, and the unicycle, started at $x_0 = 0$, is driven on $[0,1]$ with amplitude 1. Integration by parts gives $\mathbb{A}(Y_n) = A_n + \int_0^1 X_n^2(t)\,dt$. For this motif $\mathbb{A}(Y_n) = 0.0349$ ($n=2$) and 0.0255 ($n=4$), with the limit 0.0213, i.e. the sign is opposite to that of the chord-closed loop. By Corollary 1 the prediction is $x(1)\approx\big(0,-\mathbb{A}(Y_n),0\big)$.*

Figure 2 shows the approximations labelled level 1 and level 3 (i.e. $n=2$ and $n=4$ refinements, following the numbering of the routine that generates the pre-fractal). The first column shows U^1, U^2 and the driving loop in the (U^1,U^2)-plane, the second column the motion (x_1,x_2) of the unicycle, and the third column x_1, x_2 and θ as functions of time. At $t=1$ the unicycle is back at its initial heading and has moved sideways by $x_2(1) = -0.0347$ ($n=2$) and $x_2(1) = -0.0254$ ($n=4$), in agreement with $-\mathbb{A}(Y_n) = -0.0349$ and -0.0255; the residual motion along the heading is $x_1(1) = 0.0031$ and 0.0015, respectively.

For the chord-closed loop on a short window, $U_t = \tau^{1/2}Y_n(t/\tau)$ with $\tau = 10^{-2}$, the sideways displacement agrees with $-\tau A_n$ to four digits and the relative area bias satisfies $|A-A_n|/|A| = \rho^n$ exactly, as predicted by Theorem 1(c), while the actual displacement also contains the $O(\tau^{3/2})$ log-ODE remainder; the residual motion along the heading is the $O(\tau^{3/2})$ remainder.

Fig. 2 Simulation - Unicycle



Low refinement levels suffice, but the path is wide. *The simulations show that the first refinement levels already produce the full qualitative effect, and the formulas explain why. The displacement generated by the* implemented *input is governed by the signature of the polygon that is actually used. The log-ODE prediction is therefore equally accurate for every n: above,* $x_2(1) = -0.0347$ *against* $-\mathbb{A}(Y_2) = -0.0349$*. The refinement level only decides how close this signature is to that of the limit fractal, and this distance decays geometrically, like* ρ^n *(Theorem 1). Since* A_n *is explicit, the remaining bias can even be removed by retuning* θ *for the chosen* n *(Remark 3). In practice one therefore uses a low level* n*, which keeps the input amplitudes moderate (they grow like* $M^{n(1-\alpha)}$*), while the fractal limit provides the uniform error bounds.*

However, the net displacement is small compared with the region the unicycle sweeps to produce it. This is the price one pays for moving in the bracket direction. In Figure 2 the net sideways shift is $|x_2(1)| \approx 0.03$*. To produce it, the unicycle moves back and forth along its heading over the whole range* $x_1 \in [-0.1, 0.1]$*, a band about seven times longer than the shift itself. The refinement level does not change this. The back-and-forth strokes are the level-1 part* U^1 *of the driver, whose size* $\tau^\alpha \sup_t |Y_t^1|$ *is the same for every* n *The back-and-forth strokes are the level-1 part* U^1 *of the driver, whose size is the same for every n: in Figure 2 (drift-subtracted loop,* $\tau = 1$*) they fill* $x_1 \in [-0.1, 0.1]$*, and for the chord-closed loop with* $\tau = 10^{-2}$ *the excursion along the*

heading is $\tau^{1/2}\sup_t|Y^1_t| = 0.0999$ *for* $n = 1,\dots,5$. *Refinement only adds finer wiggles on top (Proposition 2). Moreover, the ratio between the width of the band and the net shift, of order* $\tau^\alpha/\tau^{2\alpha} = \tau^{-\alpha}$, *grows as the window shrinks. To obtain a narrow path one has to repeat the loop instead. With* K *loops of length* τ/K, *the net shift* τA_n *is unchanged, while the width of the band decreases like* $(\tau/K)^{1/2}$ *(Proposition 3). The motion then converges to the straight sideways segment, at the cost of* K *times more switching of the inputs.*

Example 3.5 (Unicycle: repeated loops)**.** *For the unicycle,* $[V_1,V_2](x) = (\sin x_3, -\cos x_3, 0)^\top$ *does not change the heading. The bracket curve is therefore the straight segment*

$$z_t = x_0 + t\,A\,(\sin\theta_0, -\cos\theta_0, 0)^\top, \qquad t\in[0,\tau],$$

perpendicular to the initial heading. By Proposition 3, the (x_1,x_2)*-trajectory lies in a tube of radius* $C(\tau/K)^{1/2}$ *around this segment, and the tube shrinks to the segment as* $K\to\infty$. *The picture is explicit, because the unicycle can be integrated in closed form. With* $\zeta = x_1 + ix_2$ *and* $\theta_t = \theta_0 + U^2_{0,t}$,

$$\zeta_t - \zeta_0 = e^{i\theta_0}\int_0^t e^{iU^2_{0,s}}\,dU^1_s = e^{i\theta_0}\Big(U^1_{0,t} + i\int_0^t U^2_{0,s}\,dU^1_s + R_t\Big), \qquad |R_t| = O\big(|U|^2_\infty\,|U^1|\big).$$

Along the heading, the unicycle performs the back-and-forth strokes $U^1_{0,t}$, *of size* $(\tau/K)^{1/2}$. *Transversally, it accumulates the running area* $\int U^2\,dU^1$, *which equals* $-\mathbb{A}$ *after each closed loop.* Numerical check *(motif of Example 3.2, chord-closed loop,* $n=4$, $\tau=1$*): for* $K = 1, 4, 16, 64, 256$, *the maximal distance of* (x_1,x_2) *from the segment is* $0.993,\ 0.499,\ 0.250,\ 0.125,\ 0.0625$. *This agrees with* $K^{-1/2}\sup|Y^1| = K^{-1/2}$ *within* 1% *(to three digits for* $K\ge 4$*). The end point error along the heading is* $7.6\cdot 10^{-3}K^{-1/2}$, *in agreement with (i). By contrast, for a single loop (*$K=1$, $\tau = 10^{-2}$*), the excursion along the heading is* 0.0999 *for every* $n = 1,\dots,5$. *It does not shrink with the level, while the end point converges to* $-\tau A$ *with relative bias* ρ_2^n.

Motif-level area profile

For completeness we describe the whole function $t\mapsto\mathbb{A}(t) := \mathbb{A}_{0,t}$ of the fractal X; note $\mathbb{A}(0)=0$ and $\mathbb{A}(1)=A$. Let $t\in I_k = [{}^{k-1}\!/_M, {}^{k}\!/_M]$ and let $t_1 := Mt-(k-1)\in[0,1]$ be the local time in the k-th child. By Chen's identity at the point ${}^{k-1}\!/_M$, by the similarity invariance of the area (fact (i) in Section 3.4) and since the k-th child is $F_k\circ X$ run at speed M,

$$\mathbb{A}(t) = \mathbb{A}\big(\tfrac{k-1}{M}\big) + \tfrac12\,w_{k-1}\wedge\big(r_kR(a_k)X(t_1)\big) + r_k^2\,\mathbb{A}(t_1), \qquad \mathbb{A}\big(\tfrac{k-1}{M}\big) = A\sum_{l<k}r_l^2 + \tfrac12\sum_{1\le i<j\le k-1} v_i\wedge v_j,$$

with the partial sums $w_{k-1} = v_1+\cdots+v_{k-1}$ from (3.3). Iterating along the M-adic digits of t evaluates $\mathbb{A}(t)$ to any accuracy; after n steps the remaining error is at most $(\max_k r_k^2)^n\sup_s|\mathbb{A}(s)|$.

4 Beyond level 2: higher levels and convergence

Let us investigate what happens when we want to generate higher-order Lie brackets. To illustrate this, we introduce the following example.

Example 4.1. *We consider the* car with one trailer *model with state*

$$Z = (x, y, \theta, \phi) \in \mathbb{R}^4,$$

where (x, y) is the position of the car, θ its heading, and $\phi = \theta - \theta_1$ the hitch angle between the car and the trailer (heading θ_1). The rolling constraint of the trailer, $\dot{\theta}_1 = {}^{u_1}/_{d} \sin(\theta - \theta_1)$, gives $\dot{\phi} = u_2 - {}^{u_1}/_{d} \sin\phi$; we normalise the trailer length to $d = 1$ (see, e.g., [3]). The control inputs are $u = (u_1, u_2)$, and the dynamics read

$$\begin{aligned} &\dot{x}(t) = u_1(t)\cos\theta(t),\ \dot{y}(t) = u_1(t)\sin\theta(t), \\ &\dot{\theta}(t) = u_2(t),\ \dot{\phi}(t) = -u_1(t)\sin\phi(t) + u_2(t). \end{aligned}$$

This can be written in driftless control form $\dot{Z}(t) = u_1(t)V_1(Z(t)) + u_2(t)V_2(Z(t))$, with vector fields

$$V_1(Z) = \begin{pmatrix} \cos\theta \\ \sin\theta \\ 0 \\ -\sin\phi \end{pmatrix}, \qquad V_2(Z) = \begin{pmatrix} 0 \\ 0 \\ 1 \\ 1 \end{pmatrix}.$$

The distribution at $Z = (0,0,0,0)^\top$

$$\Delta(Z) = \operatorname{span}\{V_1(Z), V_2(Z)\}$$

has rank $2 < 4$, so the control vector fields do not span the full tangent space instantaneously. Non-holonomy is seen from the failure of this distribution to be integrable: Lie brackets generate directions outside Δ. Let us calculate the first Lie brackets. Since V_2 is constant, $J_{V_2} = \mathbf{0}$, and

$$[V_1, V_2] = -J_{V_1} \cdot V_2.$$

The Jacobian of V_1 with respect to $Z = (x, y, \theta, \phi)$ is

$$J_{V_1}(Z) = \begin{pmatrix} 0 & 0 & -\sin\theta & 0 \\ 0 & 0 & \cos\theta & 0 \\ 0 & 0 & 0 & 0 \\ 0 & 0 & 0 & -\cos\phi \end{pmatrix}.$$

Multiplying by $V_2(Z) = (0,0,1,1)^\top$ *yields*

$$J_{V_1}(Z)\cdot V_2(Z) = \begin{pmatrix} -\sin\theta \\ \cos\theta \\ 0 \\ -\cos\phi \end{pmatrix}, \quad \textit{and hence} \quad \Rightarrow [V_1,V_2](Z) = \begin{pmatrix} \sin\theta \\ -\cos\theta \\ 0 \\ \cos\phi \end{pmatrix}.$$

This bracket generates a lateral motion in (x,y) *together with a* ϕ*–component. Let* $W = [V_1,V_2]$*. Its components are*

$$W^1(Z) = \sin\theta, \quad W^2(Z) = -\cos\theta, \quad W^3(Z) = 0, \quad W^4(Z) = \cos\phi.$$

The Jacobian of W *is*

$$J_W = \begin{pmatrix} 0 & 0 & \cos\theta & 0 \\ 0 & 0 & \sin\theta & 0 \\ 0 & 0 & 0 & 0 \\ 0 & 0 & 0 & -\sin\phi \end{pmatrix}.$$

We compute now $[V_1,W] = J_W\cdot V_1 - J_{V_1}\cdot W$*. First, we get*

$$J_W\cdot V_1(Z) = \begin{pmatrix} 0 \\ 0 \\ 0 \\ \sin^2\phi \end{pmatrix}, \; J_{V_1}\cdot W(Z) = \begin{pmatrix} 0 \\ 0 \\ 0 \\ -\cos^2\phi \end{pmatrix}.$$

Therefore, we obtain

$$[V_1,[V_1,V_2]](Z) = \begin{pmatrix} 0 \\ 0 \\ 0 \\ \sin^2\phi + \cos^2\phi \end{pmatrix} = \begin{pmatrix} 0 \\ 0 \\ 0 \\ 1 \end{pmatrix}.$$

We now obtain all directions; in particular, at $Z_0 = (0,0,0,0)^\top$ *we have*

- $V_1(Z_0) = e_1$ *and* $V_2(Z_0) = e_3 + e_4$*;*
- $[V_1,V_2](Z_0) = -e_2 + e_4$*, which adds the lateral* y*-direction (together with a* ϕ*-component);*
- $[V_1,[V_1,V_2]](Z_0) = e_4$*, which yields the independent* ϕ*-direction, since* $e_4 \notin \operatorname{span}\{V_1,V_2,[V_1,V_2]\}(Z_0)$*;*
- $[V_2,[V_1,V_2]](Z) = J_W V_2 = (\cos\theta,\sin\theta,0,-\sin\phi)^\top$*, hence* $[V_2,[V_1,V_2]](Z_0) = e_1 \neq 0$*;*
- *finally,* $J_{V_1}V_1(Z) = (0,0,0,\sin\phi\cos\phi)^\top$ *and* $J_{V_2}V_2(Z) = (0,0,0,0)^\top$*.*

Here e_i *is the* i*-th unit vector in* $\mathbb{R}^4$*. Hence, the Lie algebra rank condition holds, and the car–trailer system is locally accessible, even at* $Z_0 = (0,0,0,0)^\top$*.*

Let us analyse the log-ODE (generalised Magnus) expansion. Our stacked system on $\mathbb{R}^4$ driven by the controlled vector fields V_1 and V_2 reads

$$dZ_t = \sum_{i=1}^{2} V_i(Z_t)\, dU_t^i, \tag{4.1}$$

where the control paths U^i are absolutely continuous, $U_t^i = \int_0^t u_i(s)\, ds$. For $i \in \{1,2\}$ define the level-1 components $U_{s,t}^{(1),i} = U_t^i - U_s^i$, for $i,j \in \{1,2\}$ we define the Lévy areas induced by the controls on $[s,t]$ by

$$\mathbb{A}_{s,t}^{1,2} := \frac{1}{2}\int_s^t \left(U_{s,r}^{(1),1}\, dU_r^{(1),2} - U_{s,r}^{(1),2}\, dU_r^{(1),1}\right). \tag{4.2}$$

The Lévy area is the antisymmetric part of the level-2 signature of the control path.

Let us consider the log-ODE expansion of (4.1), which has no drift, assuming that V_1, V_2 are C_b^γ-vector fields on $\mathbb{R}^4$ with $\gamma > p$. Then, for $0 \le s < t \le T$, the associated flow $\Phi_{s,t}$ satisfies the log–ODE expansion

$$\begin{aligned} \log \Phi_{s,t} &= \sum_{i=1}^{2} V_i\, U_{s,t}^{(1),i} + [V_1, V_2]\, \mathbb{A}_{s,t}^{1,2} \\ &\quad + \sum_{i=1}^{2} [V_i, [V_1, V_2]]\, \ell_{s,t}^{i,(1,2)} + O\big(\omega(s,t)^{4/p}\big), \end{aligned} \tag{4.3}$$

with $\ell_{s,t}^{i,(1,2)}$ given by (1.10). Let $\mathbf{U}$ be a geometric rough path of finite p-variation with $p \in [3,4)$ (e.g. $p = 1/\beta$ with e.g. $p = 1/\beta$ with $\beta \in (\frac{1}{4}, \frac{1}{3})$ as in Theorem 1. In particular,

$$\mathbf{U}_{s,t} = \big(U_{s,t}^{(1)}, U_{s,t}^{(2)}, U_{s,t}^{(3)}\big), \qquad 0 \le s \le t \le T,$$

where

$$U_{s,t}^{(1)} \in \mathbb{R}^2, \quad U_{s,t}^{(2)} \in (\mathbb{R}^2)^{\otimes 2}, \quad U_{s,t}^{(3)} \in (\mathbb{R}^2)^{\otimes 3},$$

such that Chen's relation and the geometricity conditions are satisfied. By Proposition 1 and the brackets computed in Example 4.1, the time-one map of the log-ODE at $Z_0 = (0,0,0,0)^\top$ gives

$$\begin{aligned} \Phi_{0,t}(Z_0) - Z_0 = e_1\, U_{0,t}^{(1),1} + (e_3 + e_4)\, U_{0,t}^{(1),2} + (-e_2 + e_4)\, \mathbb{A}_{0,t}^{12} + \big(\text{non-Lie terms, vanishing if } U_{0,t}^{(1)} = 0\big) \\ + e_4\, \ell_{0,t}^{1,(1,2)} + e_1\, \ell_{0,t}^{2,(1,2)} + O\big(\omega(0,t)^{4/p}\big), \end{aligned}$$

since $[V_1,[V_1,V_2]](Z_0) = e_4$ and $[V_2,[V_1,V_2]](Z_0) = e_1$. Note that the coefficients of e_4 and e_1 are the log-signature coefficients (1.10), not raw third-level entries.

4.1 How to set up a motif

We now construct a rough driver for Example 4.1. To generate motion in the ϕ-direction at $(0,0,0,0)^\top$, we need

- $U_{0,1}^{(1),1} = U_{0,1}^{(1),2} = 0$;
- $\mathbb{A}_{0,1}^{1,2} = 0$;
- $\ell_{0,1}^{1,(1,2)}$ as large as possible;
- $\ell_{0,1}^{2,(1,2)} = 0$.

The first two conditions are the hypotheses of Corollary 1(b): they switch off level 1 and the Lévy area, so that the leading contribution to the displacement is the degree-3 term. Since *both* degree-3 directions are active at Z_0 ($[V_1,[V_1,V_2]](Z_0) = e_4$, $[V_2,[V_1,V_2]](Z_0) = e_1$), a pure ϕ-motion also requires the last condition; otherwise the trailer additionally moves by $\ell_{0,1}^{2,(1,2)}$ along the x-axis. Let us start with $M = 5$, and

$$(a_1,\dots,a_5) = (0,\theta,-2\theta,\theta,0),$$
$$(r_1,\dots,r_5) = (c,b,d,b,c).$$

Closure and regularity. The vertical part of the chord condition (3.2) reads $2b\sin\theta = d\sin(2\theta)$, i.e. $b = d\cos\theta$; the horizontal part gives

$$c = \tfrac{1}{2}\big(1 - 2b\cos\theta - d\cos(2\theta)\big).$$

Since $d > b$, the longest segment is the middle one, and Hölder regularity $\alpha = 1/3$ requires $d = r_{\max} = 5^{-1/3} \approx 0.585$ (not $b \sim M^{-1/3}$). The constraint $0 < c \le d$ restricts θ to $(0.604, 1.136)$.

Level 2. The motif is a palindrome: the sequence of directions and lengths is the same when read backwards. Hence the motif, and every pre-fractal, is symmetric under the point reflection $x \mapsto e_1 - x$ combined with time reversal. Time reversal changes the sign of the Lévy area and the rotation by π preserves it, so $A_1 = 0$ and therefore $A_n = 0$ for all n and $A = 0$ *for every* θ. The condition $\mathbb{A}_{0,1}^{12} = 0$ is thus automatic. The condition $\mathbb{A}_{0,1}^{12} = 0$ is thus automatic.

Level 3. Since $A_1 = 0$, Lemma 2(3) applies: the level-3 signatures of the pre-fractals satisfy the affine recursion $X_{n+1;0,1}^{(3)} = T_3 X_{n;0,1}^{(3)} + C_3$ with $\|T_3\| \le \rho_3 = 2c^3 + 2b^3 + d^3 < 1$, where C_3 collects the terms of (3.9) built from levels 1 and 2 only. The limit $X_{0,1}^{(3)} = (I - T_3)^{-1} C_3$ is an explicit solution of an 8×8 linear system. For the loop Y (fractal followed by the return chord) one has $Y_{0,1}^{(1)} = 0$, $Y_{0,1}^{(2)} = 0$ and $Y_{0,1}^{(3)} = X_{0,1}^{(3)} - \frac{1}{6} e_1^{\otimes 3}$, so that $\ell^{1,(1,2)} = Y_{0,1}^{112}$ and $\ell^{2,(1,2)} = -Y_{0,1}^{122}$. For $\theta = 0.7$ we get $c = 0.1082$, $b = 0.4473$, $d = 0.5848$, $\rho_2 = 0.766$, $\rho_3 = 0.382$ and

$$\ell^{1,(1,2)} = Y_{0,1}^{112} = 0.01862, \qquad \ell^{2,(1,2)} = -Y_{0,1}^{122} = -0.01496$$

(the ratios $Y^{112} : Y^{121} : Y^{211} = 1 : -2 : 1$ confirm that $Y^{(3)}_{0,1}$ is a Lie element). The largest value of $\ell^{1,(1,2)}$ in the admissible range is 0.0353 at $\theta \to 0.604$, where $c \to 0$.

Removing the e_1-component. Let $\bar{Y}$ be the loop Y reflected at the horizontal axis ($y \mapsto -y$) and run backwards in time. Reflection changes the sign of every word with an odd number of letters 2, and time reversal changes the sign of the whole level 3 (levels 1 and 2 being zero). Hence $\bar{Y}^{112} = Y^{112}$ and $\bar{Y}^{122} = -Y^{122}$, and the concatenation $Y * \bar{Y}$ is a loop with vanishing levels 1 and 2 and

$$\ell^{1,(1,2)}(Y * \bar{Y}) = 2\, Y^{112}_{0,1}, \qquad \ell^{2,(1,2)}(Y * \bar{Y}) = 0.$$

It therefore satisfies all four conditions above. The values of $\ell^{1,(1,2)}$ and $\ell^{2,(1,2)}$ are exact: they follow from a linear system. Since the areas vanish, the level-3 part of Chen's identity (3.9) gives the affine recursion

$$X^{(3)}_{n+1;0,1} = T_3\, X^{(3)}_{n;0,1} + C_3, \qquad T_3 = \sum_{k=1}^{M} r_k^3\, R(a_k)^{\otimes 3},$$

where T_3 is a linear map on $(\mathbb{R}^2)^{\otimes 3} \cong \mathbb{R}^8$ and the constant term collects the contributions of levels 1 and 2 of the pieces; it can be read off from the motif polygon itself,

$$C_3 = S^{(3)}(\text{motif polygon}) - \tfrac{1}{6} \sum_{k=1}^{M} v_k^{\otimes 3},$$

with $S^{(3)}$ the level-3 signature of the polygon with the edges $v_1, \dots, v_M$, computed by Chen's identity. Since $\|T_3\| \le \rho_3 < 1$, the limit $X^{(3)}_{0,1}$ is the unique solution of

$$(I - T_3)\, X^{(3)}_{0,1} = C_3,$$

an 8×8 linear system. Solving it (in closed form, or numerically to machine precision, as for the values above) and using $Y^{(3)}_{0,1} = X^{(3)}_{0,1} - \frac{1}{6} e_1^{\otimes 3}$ gives $\ell^{1,(1,2)} = Y^{112}_{0,1}$ and $\ell^{2,(1,2)} = -Y^{122}_{0,1}$. For the pre-fractals, $X^{(3)}_{n;0,1}$ is obtained by iterating the recursion n times from the straight segment, $X^{(3)}_{0;0,1} = \frac{1}{6} e_1^{\otimes 3}$.

Example 4.2 (Simulation)**.** *We drive the car with trailer from $Z_0 = 0$ by $U_t = \tau^{1/3}\, L_n(t/\tau)$, where L_n is either the loop Y_n or the symmetrised loop $Y_n * \bar{Y}_n$ for the seven-segment motif of Example 4.3 ($\theta = 1.3$, $b = 0.40$); the ODE is integrated segment by segment (RK4). By Corollary 1(b) and Corollary 2(iii), the prediction is $Z_\tau \approx (\ell_n^{2,(1,2)}, 0, 0, \ell_n^{1,(1,2)})$, with the coefficients of the scaled pre-fractal loop. The single loop Y_n moves the trailer in the ϕ- and in the x-direction, the latter exactly as predicted by $\ell^{2,(1,2)}$; the symmetrised loop produces a pure ϕ-motion. The difference between simulated and predicted $\phi(\tau)$ is the $O(\tau^{4/3})$ remainder of Corollary 2(iii): it decreases from $8.8 \cdot 10^{-5}$ to $3.9 \cdot 10^{-6}$ when τ decreases by the factor 10, i.e. by $\approx 10^{4/3}$. Relative to the main term it is only $O(\tau^{1/3})$ (11% at $\tau = 10^{-2}$, 5% at $\tau = 10^{-3}$).*

loop	τ	n	$\phi(\tau)$ simulated	$\phi(\tau)$ predicted	$x(\tau)$ simulated / predicted
Y_n	10^{-2}	4	$4.283 \cdot 10^{-4}$	$3.845 \cdot 10^{-4}$	$-1.341 \cdot 10^{-4}$ / $-1.341 \cdot 10^{-4}$
$Y_n * \bar{Y}_n$	10^{-2}	3	$8.502 \cdot 10^{-4}$	$7.633 \cdot 10^{-4}$	$< 10^{-15}$ / 0
$Y_n * \bar{Y}_n$	10^{-2}	4	$8.566 \cdot 10^{-4}$	$7.690 \cdot 10^{-4}$	$< 10^{-15}$ / 0
$Y_n * \bar{Y}_n$	10^{-3}	4	$8.085 \cdot 10^{-5}$	$7.690 \cdot 10^{-5}$	$< 10^{-15}$ / 0

Table 1 Car with trailer driven by the pre-fractal loops of the seven-segment motif ($\theta = 1.3$, $b = 0.40$, $\alpha = 1/3$); $y(\tau)$ and $\theta(\tau)$ vanish up to rounding ($< 10^{-15}$).

Example 4.3 (Two-bump motif with seven segments)**.** *The figures below use a motif with $M = 7$ segments and two bumps, one up and one down,*

$$(a_1, \dots, a_7) = (0, \theta, -\theta, 0, -\theta, \theta, 0), \qquad (r_1, \dots, r_7) = (c, b, b, e, b, b, c),$$

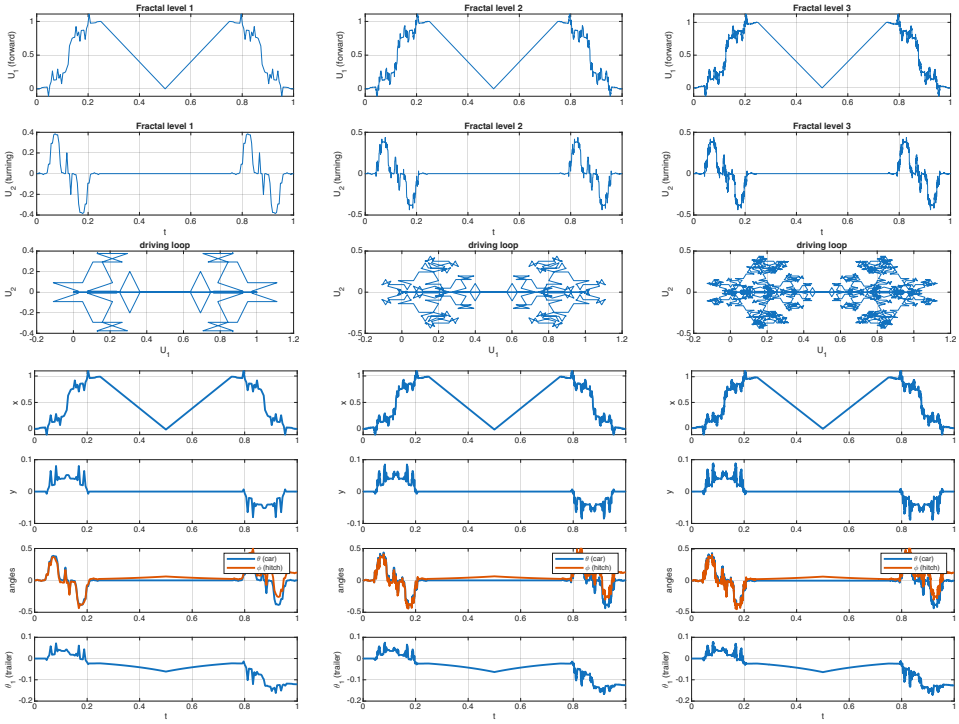
with $\theta = 1.3$, $b = 0.40$, the flat middle segment $e = 7^{-1/3} \approx 0.5228$ as the longest one (so that $\alpha = 1/3$), and $c = 1/2(1 - e - 4b\cos\theta) = 0.0246$ from the chord condition. The motif is a palindrome, hence all pre-fractals have zero Lévy area; moreover $\rho = \sum_k r_k^2 = 0.914 < 1$ and $\rho_3 = 0.399$. The limit coefficient is $\ell^{1,(1,2)} = 0.0385$, about twice the value of the five-segment motif above. The car with trailer is driven on $[0, 1]$ with amplitude 1 by the symmetrised loop $Y_n * \bar{Y}_n$ (closed along the chord) for $n = 2, 3, 4$ (labelled level 1, 2, 3 in the figures). The first three rows show U^1, U^2 and the driving loop, the remaining rows x, y, the angles θ and ϕ, and the heading $\theta_1 = \theta - \phi$ of the trailer. At $t = 1$ the car is back at its initial position and heading ($x, y, \theta \approx 10^{-16}$), while the trailer has turned:

$$\phi(1) = -\theta_1(1) = 0.1210, \quad 0.1254, \quad 0.1264 \qquad (n = 2, 3, 4),$$

so already for $n = 2$ the displacement is only about 4% smaller than for $n = 4$. During the manoeuvre θ and ϕ almost coincide, since both are driven by u_2; only their difference $-\theta_1$, which obeys $\dot{\theta}_1 = u_1 \sin\phi$, accumulates the third-order effect. Because the loop is not small, the third-order prediction $2\ell_n^{1,(1,2)} = 0.074,\ 0.076,\ 0.077$ underestimates the displacement by about 40%; for amplitude κ the prediction scales like κ^3 and the error like κ^4, cf. Table 1.

The figures below use a motif seven-segment motif ($\theta = 1.3$, $b = 0.40$) for $n = 2, 3, 4$.

Fig. 3 The trailer



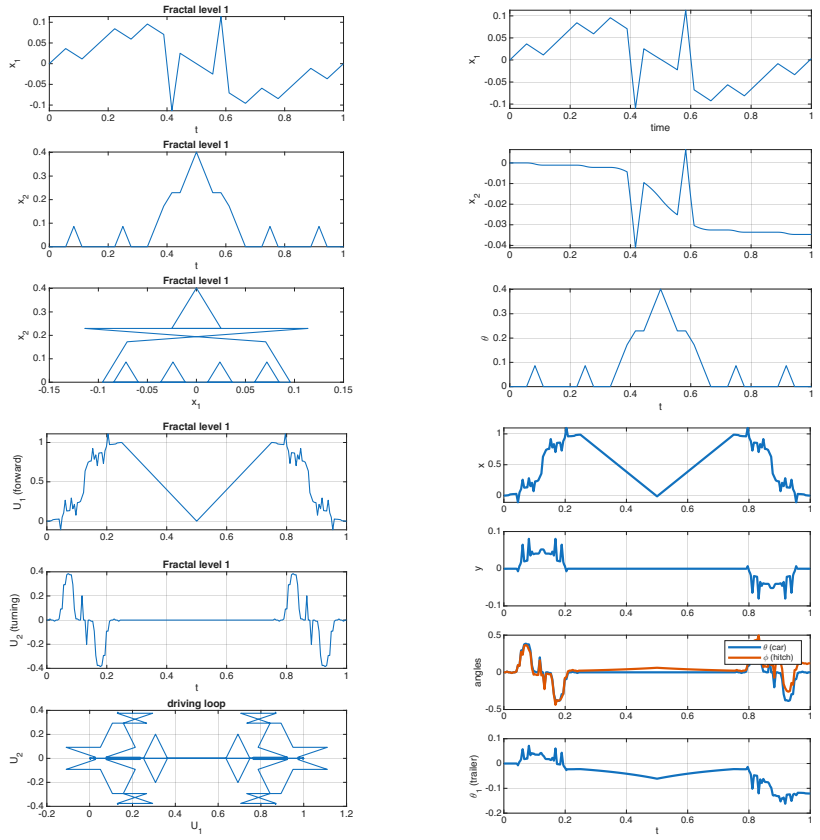
5 Conclusion and outlook: rough paths and fractals as a design tool in control theory

The examples above illustrate how ideas from *rough path theory* can enrich classical nonlinear control. Traditionally, controllability in driftless systems relies on smooth concatenations of controls that exploit the system's Lie algebra structure: alternating inputs along V_1, V_2 produce a net motion in the commutator direction $[V_1, V_2]$. This mechanism underlies the Chow–Rashevskii theorem; constructive implementations based on concatenated or oscillatory controls typically require careful timing and cancellation.

By contrast, fractal Koch-type inputs encode these higher-order commutator effects explicitly through their iterated integrals, which are computable in closed form from the motif (Lemma 1, Lemma 2). In Lyons' rough differential framework, the signature $(X^{(1)}, X^{(2)}, X^{(3)}, \dots)$ of a control path $\mathbf{X}$ carries exactly the geometric data needed to reproduce motions along all Lie brackets. Thus, by *designing* a rough path with prescribed first and second (or higher) signature levels, one can directly program small displacements in specific bracket directions. The implementable pre-fractal

inputs inherit this property with an explicit, geometrically decaying bias (Theorem 1, Corollary 2), as confirmed by the simulations in Examples 3.4 and 4.2.

Fig. 4 Low-level and repeated controls: the first row illustrates the unicycle of Example 3.3, and the second row the car-with-trailer system of Example 4.1.



Low refinement levels and repetition. The simulations suggest a simple practical strategy: use a pre-fractal of level n and repeat it. The pre-fractal of level n has M^n segments and is computed recursively. Low levels are obtained almost instantly and keep the input amplitudes moderate (Remark 3). A higher level n reduces the area bias ρ_2^n, but it does not make the path narrower: the width of the swept band is set by the level-1 part of the driver and is independent of n. A narrow path is obtained instead by repeating the loop K times within the window (Proposition 3). The log-ODE approximation applies to the polygon that is actually implemented; the refinement level primarily controls how closely its signature approximates that of the limiting fractal. In particular, the displacement is determined by the signature of the polygon

actually used, and the distance to the fractal limit decays like ρ^n. Repeating a closed loop K times multiplies the effect: exactly by K for the unicycle, and approximately for the car with trailer. The fractal limit itself provides the uniform error bounds of Theorem 1 and Corollary 2. See Figure 4.

More broadly, this approach suggests a new synthesis between rough path analysis and control design. Rough paths provide a rigorous calculus for irregular signals - bridging deterministic control, rough forcing, and fractal geometry. By prescribing the signature of a control path, one gains access not only to classical Lie bracket motions but also to higher-order directions that are otherwise difficult to realise smoothly. Such ideas suggest further possibilities for structured small-scale steering with explicitly designed rough input patterns.

In summary, rough paths transform geometric control from a qualitative existence theory into a quantitative design tool: they allow one to construct explicit, tunable, and reproducible control signals whose algebraic structure directly realises the desired motion in the system's Lie algebra.

Acknowledgements. Erika Hausenblas was supported by the Austrian Science Fund, Project P32295. Kistosil Fahim and Erika Hausenblas were supported by the Federal Ministry of Education, Science and Research (BMBWF) through ASEA-UNINET. Erika Hausenblas was also supported by the Sydney Mathematical Research Institute (SMRI) and thanks the institute for its hospitality.

Declarations

Funding. This work was supported by the Austrian Science Fund (FWF), Project P32295 (Erika Hausenblas), and by the Austrian Federal Ministry of Education, Science and Research (BMBWF) through ASEA-UNINET (Kistosil Fahim and Erika Hausenblas). Erika Hausenblas was also supported by the Sydney Mathematical Research Institute (SMRI).

Competing interests. The authors declare that they have no competing interests.

Ethics approval and consent to participate. Not applicable.

Consent for publication. Not applicable.

Data availability. Data sharing is not applicable to this article, as no datasets were generated or analysed during the current study.

Materials availability. Not applicable.

Code availability. The code used to generate the numerical illustrations (figures) is available from the corresponding author on reasonable request.

Author contribution. All authors contributed to the conception of the study, the mathematical analysis, the construction of the examples, and the writing of the manuscript. All authors read and approved the final manuscript.

Appendix A Rough paths — a short introduction

This section is intended for researchers from control theory who are not familiar with rough path theory. We summarise the objects needed in this paper: geometric rough paths (Hölder and p-variation viewpoints), and rough differential equations (RDEs) with the log-ODE expansion. The aim is to justify rigorously how our fractal (Koch-type) drivers define integrals and flows beyond the Young regime. Introductory references on rough path theory include Lyons [7], Lyons–Qian [8], Friz–Victoir [9], and Friz–Hairer [10].

The Motivation

We consider an ordinary differential equation (ODE) driven by a possibly irregular signal

$$dz_t = \sum_{i=1}^{m} V_i(z_t)\, dX_t^i, \qquad z_0 \in \mathbb{R}^d, \tag{A1}$$

where $V_1, \dots, V_m : \mathbb{R}^d \to \mathbb{R}^d$ are sufficiently smooth vector fields and $\mathbf{X} = (X_t^1, \dots, X_t^m)$ is a given driving signal defined on the interval $[0, T]$.

When the paths $[0, T] \ni t \mapsto X_t^i$ are not differentiable in the classical sense but possess a sufficiently large Hölder exponent, the differential equation above is interpreted in the sense of Young integration.

Let $f : [0, T] \to \mathbb{R}^{n\times d}$ be α-Hölder continuous and $X : [0, T] \to \mathbb{R}^d$ be β-Hölder continuous, that is,

$$\|f\|_\alpha = \sup_{s\neq t} \frac{|f_t - f_s|}{|t-s|^\alpha} < \infty, \quad \|X\|_\beta = \sup_{s\neq t} \frac{|X_t - X_s|}{|t-s|^\beta} < \infty.$$

The celebrated **Young theorem** states that if $\alpha + \beta > 1$, then the Riemann–Stieltjes integral

$$\int_s^t f\, dX \;=\; \lim_{|\pi|\to 0} \sum f_{t_i}\,(X_{t_{i+1}} - X_{t_i}) \quad \text{(level 1 only)}.$$

is well-defined as the limit of Riemann sums; see [43].The **Young theorem** states that, if $\alpha+\beta > 1$, the Riemann–Stieltjes sums $\sum_i f_{t_i}(X_{t_{i+1}} - X_{t_i})$ converge as $|\pi| \to 0$; the limit $\int_s^t f\, dX$ is the Young integral, see [43]. Moreover, there exists a constant $C_{\alpha,\beta}$ such that

$$\left| \int_s^t f_r\, dX_r - f_s(X_t - X_s) \right| \le C_{\alpha,\beta}\, \|f\|_\alpha \|X\|_\beta |t-s|^{\alpha+\beta}.$$

However, when the driving signal X is too irregular, the condition $\alpha + \beta > 1$ may fail. For example, if X has Hölder regularity $\gamma < 1/2$ (as in the case of Brownian motion, where γ can be taken arbitrarily close to $1/2$), then the Young integral is no longer well-defined for generic integrands of similar regularity. This breakdown occurs precisely when

$$\alpha + \beta \le 1.$$

In this regime, higher-order information about the path X is required in order to make sense of such integrals. Specifically, if $\alpha \in (1/3, 1/2]$ and the second level $X^{(2)}$ of the driving signal is given, the solution z_t of (A1) admits the Chen–Fliess (Taylor-type) expansion (1.5) at z_0,

$$z_t = z_0 + \sum_i X^i_{0,t}\, V_i(z_0) + \sum_{i,j} X^{ij}_{0,t}\, \big(DV_j\, V_i\big)(z_0) + \cdots,$$

where the remainder is of order $t^{3\alpha}$.

As mentioned in the introduction, one can include higher-order iterated integrals. The level-k component of the truncated signature has the form

$$X^{(k),(i_1,\cdots,i_k)}_{s,t} = \int_{s<r_1<\cdots<r_k<t} dX^{i_1}_{r_1} \cdots dX^{i_k}_{r_k}.$$

As in (1.6), the second-order term is a bracket term only after the symmetric part $\operatorname{Sym} X^{(2)}_{0,t} = 1/2 X^{(1)}_{0,t} \otimes X^{(1)}_{0,t}$ has been separated; it is not admissible to write it directly as a Lie bracket. These iterated integrals naturally arise in the algebraic and geometric study of differential equations driven by rough paths and provide the foundation for rough path theory.

The definition of rough paths

Before introducing rough paths, let us introduce some definitions: For a continuous path $X : [0,T] \to \mathbb{R}^d$ and $p \in [1,\infty)$, its p-variation on $[s,t] \subset [0,T]$ is

$$\|X\|_{p\text{-var};[s,t]} := \left(\sup_{\Pi} \sum_i |X_{t_i,t_{i+1}}|^{\,p} \right)^{1/p}, \tag{A2}$$

where the supremum runs over all partitions $\Pi :\ s = t_0 < \cdots < t_n = t$ and $X_{t_i,t_{i+1}} = X_{t_{i+1}} - X_{t_i}$.

Remark 5. If X is α-Hölder on $[s,t]$, $|X_t - X_s| \le C_\alpha |t-s|^\alpha$, then for any $p > 1/\alpha$,

$$\|X\|_{p\text{-var};[s,t]} = \Big(\sup_{\Pi} \sum_i |X_{t_{i+1}} - X_{t_i}|^p \Big)^{1/p} \le C_\alpha\, |t-s|^\alpha.$$

Conversely, finite p-variation alone does not imply $1/p$-Hölder regularity. However, if there exist $\theta > 0$ and C with $\operatorname{Var}_p(X;[s,t])^p \le C|t-s|^\theta$ for all $s < t$, then

$$|X_t - X_s| \le \operatorname{Var}_p(X;[s,t]) \le C^{1/p} |t-s|^{\theta/p},$$

so X is Hölder with exponent $\alpha = \theta/p$.

We now have all the necessary ingredients to define a rough path.

Definition 5 (Geometric p-rough path)**.** Let $p \in [1, \infty)$ and set $N = \lfloor p \rfloor$. A *p-rough path* over $\mathbb{R}^d$ is an irregular path $X : [0, T] \to \mathbb{R}^d$ together with an *enhancement*

$$\mathbf{X}_{s,t} = \big(X^{(1)}_{s,t}, X^{(2)}_{s,t}, \dots, X^{(N)}_{s,t}\big), \qquad 0 \le s < t \le T,$$

where $X^{(1)}_{s,t} = X_t - X_s \in \mathbb{R}^d$, and $X^{(k)}_{s,t} \in (\mathbb{R}^d)^{\otimes k}$ for $k = 2, \dots, N$ is given by the iterated integrals

$$X^{(k)}_{s,t} = \int_{s<u_1<\cdots<u_k<t} dX_{u_1} \otimes \cdots \otimes dX_{u_k}. \tag{A3}$$

The enhancement $\mathbf{X} = (X^{(1)}, \dots, X^{(N)})$ is a p-rough path if it satisfies the multiplicative and analytic conditions below. Weak geometricity additionally requires the increments to be group-like (equivalently, to satisfy the shuffle relations); a geometric p-rough path is a rough-path limit of signatures of smooth or bounded-variation paths.

1. **Chen's relation (multiplicativity).** For all $s \le u \le t$, $\mathbf{X}_{s,t} = \mathbf{X}_{s,u} \otimes \mathbf{X}_{u,t}$, that is, $X^{(1)}_{s,t} = X^{(1)}_{s,u} + X^{(1)}_{u,t}$, and at level 2, $X^{(2)}_{s,t} = X^{(2)}_{s,u} + X^{(2)}_{u,t} + X^{(1)}_{s,u} \otimes X^{(1)}_{u,t}$, with analogous identities for $k \le N$.
2. **Analytic p-variation bound.** There exists a control function[5] $\omega : [0, T]^2 \to [0, \infty)$, which may be chosen to measure the p-variation of $\mathbf{X}$, such that

   $$\|\mathbf{X}^{(k)}_{s,t}\| \;\lesssim\; \omega(s, t)^{k/p}, \qquad k = 1, \dots, N.$$

   This guarantees the correct scaling needed for rough integration and rough differential equations.
3. **Geometricity.** There are smooth paths X^ε whose truncated signatures $S_N(X^\varepsilon)$ converge to $\mathbf{X}$ in the p-variation rough path metric.

In the special case $p \in (2, 3)$, a (weakly) geometric p-rough path consists of $\mathbf{X} = (X, \mathbb{X})$, $\mathbb{X}_{s,t} \in (\mathbb{R}^d)^{\otimes 2}$, where the *geometric* condition is the symmetry identity $\operatorname{Sym} \mathbb{X}_{s,t} = {}^1\!/_2\, X_{s,t} \otimes X_{s,t}$. Consequently, the antisymmetric part

$$\mathbb{A}_{s,t} = {}^1\!/_2\big(\mathbb{X}_{s,t} - \mathbb{X}^\top_{s,t}\big) \tag{A4}$$

Given $\mathbf{X}$ up to level N, the rough integral $\int Y \, d\mathbf{X}$ and the RDE

$$dZ_t = \sum_{i=1}^{d} V_i(Z_t)\, d\mathbf{X}^i_t$$

are defined *pathwise* and the solution map is continuous in the rough path topology (stability under approximations, e.g., by fast oscillations). In particular, the solutions driven by the n-th polygonal approximations of the generalised Koch curve converge to the solution driven by the fractal, with the explicit rate of Theorem 1 and Corollary 2.

[5] Continuous, superadditive, with $\omega(t, t) = 0$.

In control, the level-2 area captures bracket effects ($[V_i, V_j]$); higher levels capture higher-order commutators.

Scaling under time compression

If a fixed α-Hölder pattern X on $[0,1]$ is compressed to $[0,\tau]$ by $X^\tau_t = \tau^\alpha X_{t/\tau}$, then its level-$k$ signature scales as $\tau^{k\alpha}$. In a p-variation formulation the corresponding homogeneous scaling is of order $\tau^{k/p}$.

For illustration, we formulate the Gubinelli derivative for the unicycle. For more details, see the book [10].

Example A.1. *Let $\mathbf{X} = (X, X^{(2)})$ be a step–2 geometric rough path over $\mathbb{R}^m$ (e.g. a Koch–type driver with $\alpha = 1/2$ enhanced by its Lévy area). An $\mathbb{R}^n$–valued path Z is* controlled by *X if there exists a map $Z' : [0,T] \to \mathcal{L}(\mathbb{R}^m, \mathbb{R}^n)$ (the* Gubinelli derivative*) and a remainder R^X such that, for all $s < t$,*

$$Z_t - Z_s \;=\; Z'_s\, X^{(1)}_{s,t} \;+\; R^X_{s,t}, \qquad |R^X_{s,t}| \lesssim |t-s|^{2\alpha}. \tag{A5}$$

Take $m = 2$ and the (driftless) kinematic unicycle

$$\dot{x}_1(t) = u_1(t)\cos\theta(t),\ \dot{x}_2(t) = u_1(t)\sin\theta(t),\ \dot{\theta}(t) = u_2(t),$$

and view the controls as a planar rough driver $\mathbf{X} = (X^{(1)}, X^{(2)})$ (e.g. a Koch curve with $\alpha = 1/2$ and its Lévy area). Due to (2.2), the solution $x = (x_1, x_2, \theta)$ is controlled by $\mathbf{X}$ with the explicit *Gubinelli derivative*

$$x'_t \;=\; \big[\, V_1(x_t), V_2(x_t) \,\big] \;=\; \begin{bmatrix} \cos\theta_t & 0 \\ \sin\theta_t & 0 \\ 0 & 1 \end{bmatrix}. \tag{A6}$$

Componentwise, we get for $s < t$, using (1.5) and $DV_1\, V_2 = (-\sin\theta, \cos\theta, 0)^\top$, $DV_2\, V_1 = DV_1 V_1 = DV_2 V_2 = 0$,

$$\begin{aligned} x_1(t) - x_1(s) &= \cos\theta_s X^{(1),1}_{s,t} + (-\sin\theta_s) X^{(2),21}_{s,t} \\ &\quad + O(|t-s|^{3\alpha}), \\ x_2(t) - x_2(s) &= \sin\theta_s X^{(1),1}_{s,t} + \cos\theta_s X^{(2),21}_{s,t} + O(|t-s|^{3\alpha}), \\ \theta(t) - \theta(s) &= X^{(1),2}_{s,t} + O(|t-s|^{3\alpha}). \end{aligned}$$

Here $X^{(2),21}_{s,t} = \int_s^t (X^2_r - X^2_s)\, dX^1_r$ (turning first, then driving forward). Writing $X^{(2),21}_{s,t} = 1/2 X^1_{s,t} X^2_{s,t} - \mathbb{A}^{12}_{s,t}$, the planar increment contains $\mathbb{A}^{12}_{s,t}(\sin\theta_s, -\cos\theta_s) = \mathbb{A}^{12}_{s,t}[V_1, V_2]$, which is the step–2 bracket effect.

Higher order expansion

We write $S_{s,t}$ for the (truncated) signature of X up to level $N = \lfloor p \rfloor$,

$$S_{s,t} = 1 + \sum_{k=1}^{N} X_{s,t}^{(k)}, \qquad X_{s,t}^{(k)} \in (\mathbb{R}^d)^{\otimes k},$$

and denote by $\ell_{s,t} := \log S_{s,t}$ its logarithm in the tensor algebra. Then $\ell_{s,t}$ is a *Lie series*: it takes values in the free Lie algebra generated by $e_1, \dots, e_d$, and can be written in a Hall basis [47] or in the Lyndon basis [48] of the free Lie algebra; see [16, Ch. 4–5]. In a Lie basis (e_I) it reads

$$\ell_{s,t} = \sum_{k=1}^{N} \sum_{|I|=k} \ell_{s,t}^{I} \, e_I,$$

where the scalars $\ell_{s,t}^{I}$ are universal polynomial expressions in the signature coordinates up to level k; using the shuffle identities, they can equivalently be rewritten as linear combinations of level-k word integrals. For more details see [15, 49, 50].

The log-signature and its coefficients.

For a (smooth or rough) path $X : [0, T] \to \mathbb{R}^d$, its signature over an interval $[s, t]$ is the formal series

$$S_{s,t} = 1 + \sum_{k=1}^{\infty} \sum_{|I|=k} X_{s,t}^{(k),I} \, e_{i_1} \otimes \cdots \otimes e_{i_k},$$

where $I = (i_1, \dots, i_k)$ is a word in the alphabet $\{1, \dots, d\}$ and $X_{s,t}^{(k),I}$ are the iterated integrals of order k. The signature takes values in the tensor algebra $T((\mathbb{R}^d))$ and satisfies Chen's identity $S_{s,t} = S_{s,u} \otimes S_{u,t}$.

The *log-signature* is defined as the (formal) logarithm $\ell_{s,t} := \log S_{s,t}$, which now takes values in the free Lie algebra $\mathcal{L}(\mathbb{R}^d)$ generated by $e_1, \dots, e_d$. Thus $\ell_{s,t}$ admits a Lie–series expansion

$$\ell_{s,t} = \sum_{|I|=1} \ell_{s,t}^{I} \, e_I + \sum_{|I|=2} \ell_{s,t}^{I} \, [e_{i_1}, e_{i_2}] + \sum_{|I|=3} \ell_{s,t}^{I} \, [e_{i_1}, [e_{i_2}, e_{i_3}]] + \cdots .$$

The coefficients $\ell_{s,t}^{I}$ are called the *log-signature coefficients*. For $|I| = 1$ they coincide with increments, $\ell_{s,t}^{i} = X_{s,t}^{(1),i}$. For $|I| = 2$ they recover the antisymmetric area,

$$\ell_{s,t}^{[i,j]} = \tfrac{1}{2}\big(X_{s,t}^{(2),ij} - X_{s,t}^{(2),ji}\big).$$

For $|I| \geq 3$, the coefficients $\ell_{s,t}^{I}$ are *universal polynomial expressions* in the signature coordinates (equivalently, after use of the shuffle identities, linear combinations of level-$|I|$ word integrals) obtained by applying the *Eulerian idempotent*, which projects

the tensor algebra onto the free Lie algebra. In this sense, $\ell_{s,t}$ is the canonical Lie algebra element whose exponential recovers the signature (see [51])

$$\exp(\ell_{s,t}) = S_{s,t}.$$

Appendix B Nonlinear Control Theory - a short introduction

This short appendix collects the main control-theoretic notions used implicitly throughout the paper. They form the background for interpreting rough or fractal inputs as geometrically meaningful control actions in nonlinear systems. For references in classical geometric control, we refer to *Agrachev and Sachkov* [42], *Isidori* [52], *Jurdjevic* [53], and *Sontag* [38].

A standard control system on a smooth manifold $M \subset \mathbb{R}^n$ is written in the *control-affine* form

$$\dot{x} = V_0(x) + \sum_{i=1}^{m} u_i(t)\, V_i(x),$$

where V_0 is the *drift* vector field and $V_1, \dots, V_m$ are the *control vector fields*. The input $u = (u_1, \dots, u_m)$ represents the control signal. In the driftless case ($V_0 \equiv 0$), the system is often called a *driftless system*, and motion arises solely from the directions V_i.

A *non-holonomic system* is a mechanical or control system that has velocity constraints which cannot be integrated to constraints on the positions. This means the system is allowed to move only in certain directions at each moment, but these allowed directions do not fit together to form a surface or subspace that the system must stay on. As a result, the system may reach positions that are not directly allowed by its instantaneous motion, but become reachable by combining several small motions.

Definition 6. Let M be a smooth manifold and let

$$\Delta(x) = \operatorname{span}\{V_1(x), \dots, V_m(x)\} \subset T_xM$$

be a smooth distribution generated by smooth vector fields $V_1, \dots, V_m \in \Gamma(TM)$. We say that the system

$$\dot{x}(t) = \sum_{i=1}^{m} u_i(t)\, V_i(x(t)), \qquad u(t) \in \mathbb{R}^m,$$

is *non-holonomic* if the distribution Δ is *non-integrable*, that is, if it does not arise as the tangent bundle of any family of submanifolds of M.

If the inputs switch rapidly between two directions, their infinitesimal composition yields an additional *bracket direction*. The Lie bracket of two vector fields is ($J.$ denotes the Jacobian matrix) $[V_i, V_j] = J_{V_j} V_i - J_{V_i} V_j$, and represents the leading correction in the Baker–Campbell–Hausdorff (BCH) expansion of the flow composition

$\exp(tV_i)\exp(tV_j)$. Higher nested brackets correspond to higher-order terms in this series.

When a nonzero drift V_0 is present, one includes it in the generating set of vector fields. The corresponding *Lie Algebra Rank Condition (LARC)* requires that

$$\operatorname{span}\{V_0(x), V_i(x), [V_i, V_j](x), [V_i, V_0](x), \ldots\} = T_xM.$$

Brackets of the form $[V_i, V_0]$ capture the new directions created by the interaction between the controls and the natural system dynamics.

Definition 7. We say the *Lie Algebra Rank Condition (LARC)* holds at x if $\operatorname{Lie}(x) = T_xM$. With drift, one enlarges the generating set to include V_0 and all mixed brackets $[V_0, V_i]$, $[V_i, [V_0, V_j]]$, etc., and requires $\Delta^\infty(x) := \operatorname{span}\{\, W(x) : \; W \in \operatorname{Lie}_x(V_0, V_1, \ldots, V_m)\,\} = T_xM$.

For a driftless system with smooth vector fields, if the Lie algebra generated by $\{V_i\}$ spans the tangent space at x_0, then the system is small-time locally controllable at x_0, and in particular locally accessible there. This result, known as the *Chow–Rashevskii theorem*, is the geometric cornerstone of nonlinear controllability.

Theorem 2. (see, e.g., Jurdjevic [53]) Assume $V_1, \ldots, V_m$ are real-analytic (or C^∞ and bracket-generating). If LARC holds at every point of a connected manifold M, then any two points of M can be joined by a horizontal curve (trajectory of (2.1) with $V_0 \equiv 0$). In particular, the system is *locally controllable* (hence locally accessible) at every point.

References

[1] Brockett, R.W.: Asymptotic stability and feedback stabilization. In: Brockett, R.W., Millman, R.S., Sussmann, H.J. (eds.) Differential Geometric Control Theory, pp. 181–191. Birkhäuser, Boston, MA (1983). Introduces the nonholonomic integrator and the famous "Brockett condition." Shows that some bracket-generated systems cannot be stabilized by smooth static feedback.

[2] Lizárraga, D.A.: Obstructions to the existence of universal stabilizers for smooth control systems. Mathematics of Control, Signals, and Systems **16**(3), 255–277 (2004) https://doi.org/10.1007/s00498-003-0140-x

[3] Murray, R.M., Sastry, S.S.: Nonholonomic motion planning: steering using sinusoids. IEEE Transactions on Automatic Control **38**(5), 700–716 (1993) https://doi.org/10.1109/9.277235

[4] Sussmann, H.J., Liu, W.: Limits of highly oscillatory controls and the approximation of general paths by admissible trajectories. In: Proceedings of the 30th IEEE

Conference on Decision and Control, Brighton, UK, pp. 437–442 (1991). https://doi.org/10.1109/CDC.1991.261338 . https://doi.org/10.1109/CDC.1991.261338

[5] Liu, W.: An approximation algorithm for nonholonomic systems. SIAM J. Control Optim. **35**(4), 1328–1365 (1997)

[6] Morin, P., Samson, C.: Practical stabilization of driftless systems on Lie groups: the transverse function approach. IEEE Trans. Automat. Control **48**(9), 1496–1508 (2003)

[7] Lyons, T.J.: Differential equations driven by rough signals. Rev. Mat. Iberoam. **14**(2), 215–310 (1998) https://doi.org/10.4171/RMI/240

[8] Lyons, T.J., Qian, Z.: System Control and Rough Paths. Oxford Mathematical Monographs. Oxford University Press, Oxford (2002)

[9] Friz, P.K., Victoir, N.B.: Multidimensional Stochastic Processes as Rough Paths: Theory and Applications. Cambridge Studies in Advanced Mathematics, vol. 120. Cambridge University Press, Cambridge (2010). https://doi.org/10.1017/CBO9780511845079

[10] Friz, P.K., Hairer, M.: A Course on Rough Paths: With an Introduction to Regularity Structures, 2nd edn. Universitext. Springer, Cham (2020). https://doi.org/10.1007/978-3-030-41556-3

[11] Chen, K.-T.: Integration of paths. A faithful representation of paths by non-commutative formal power series. Trans. Am. Math. Soc. **89**, 395–407 (1959) https://doi.org/10.2307/1993193

[12] Fliess, M.: Fonctionnelles causales non linéaires et indéterminées non commutatives. Bull. Soc. Math. France **109**, 3–40 (1981)

[13] Fliess, M., Lamnabhi, M., Lamnabhi-Lagarrigue, F.: An algebraic approach to nonlinear functional expansions. IEEE Trans. Circuits Syst. **30**(8), 554–570 (1983)

[14] Hairer, M., Kelly, D.: Geometric versus non-geometric rough paths. Ann. Inst. Henri Poincaré Probab. Stat. **51**(1), 207–251 (2015)

[15] Ree, R.: Lie elements and an algebra associated with shuffles. Ann. Math. **68**, 210–220 (1958)

[16] Reutenauer, C.: Free Lie Algebras. Lond. Math. Soc. Monogr., New Ser., vol. 7. Oxford University Press, Oxford (1993)

[17] Loday, J.-L.: Série de Hausdorff, idempotents eulériens et algèbres de Hopf. Expo. Math. **12**, 165–178 (1994)

[18] Strichartz, R.S.: The Campbell–Baker–Hausdorff–Dynkin formula and solutions of differential equations. Journal of Functional Analysis **72**(2), 320–345 (1987) https://doi.org/10.1016/0022-1236(87)90066-0

[19] Castell, F.: Asymptotic expansion of stochastic flows. Probability Theory and Related Fields **96**(2), 225–239 (1993) https://doi.org/10.1007/BF01192134

[20] Agrachev, A.A., Gamkrelidze, R.V.: Exponential representation of flows and chronological calculus. Math. USSR Sb. **35**(6), 727–785 (1979)

[21] Kawski, M., Sussmann, H.J.: Noncommutative power series and formal Lie-algebraic techniques in nonlinear control theory. In: Helmke, U., Prätzel-Wolters, D., Zerz, E. (eds.) Operators, Systems, and Linear Algebra, pp. 111–128. Teubner, Stuttgart (1997)

[22] Bellaïche, A.: The tangent space in sub-Riemannian geometry. In: Bellaïche, A., Risler, J.-J. (eds.) Sub-Riemannian Geometry. Progress in Mathematics, vol. 144, pp. 1–78. Birkhäuser, Basel (1996). https://doi.org/10.1007/978-3-0348-9210-0_1 . Privileged coordinates, nilpotent approximation, and Hörmander's bracket-generating condition.

[23] Montgomery, R.: A Tour of Subriemannian Geometries, Their Geodesics and Applications. Mathematical Surveys and Monographs, vol. 91. American Mathematical Society, Providence, RI (2002). https://doi.org/10.1090/surv/091 . Connects sub-Riemannian geometry with nonholonomic systems, including the Heisenberg group and rolling ball. Excellent geometric background for Lie algebra-based control. https://doi.org/10.1090/surv/091

[24] Sussmann, H.J.: A product expansion for the Chen series. In: Byrnes, C.I., Lindquist, A. (eds.) Theory and Applications of Nonlinear Control Systems, pp. 323–335. North-Holland, Amsterdam (1986)

[25] Warga, J.: Optimal Control of Differential and Functional Equations. Academic Press, New York (1972)

[26] Bressan, A., Rampazzo, F.: Impulsive control systems with commutative vector fields. Journal of Optimization Theory and Applications **81**(3), 435–457 (1994) https://doi.org/10.1007/BF00940040

[27] Silva, G.N., Vinter, R.B.: Necessary conditions for optimal impulsive control problems. SIAM J. Control Optim. **35**(6), 1829–1846 (1997) https://doi.org/10.1137/S0363012995281857

[28] Zelikin, M.I., Borisov, V.F.: Theory of Chattering Control: With Applications to Astronautics, Robotics, Economics, and Engineering. Birkhäuser, Boston (1994). https://doi.org/10.1007/978-1-4612-0265-6

[29] Bailleul, I., Diehl, J.: The inverse problem for rough controlled differential equations. SIAM J. Control Optim. **53**(5), 2762–2780 (2015)

[30] Boutaib, Y.: The accessibility problem for geometric rough differential equations. J. Dyn. Control Syst. **29**(4), 1669–1693 (2023)

[31] Bailleul, I.: Flows driven by rough paths. Revista Matemática Iberoamericana **31**(3), 901–934 (2015) https://doi.org/10.4171/rmi/858

[32] Diehl, J., Friz, P.K., Gassiat, P.: Stochastic control with rough paths. Appl. Math. Optim. **75**(2), 285–315 (2017) https://doi.org/10.1007/s00245-016-9333-9

[33] Nishimura, Y.: Quasi-optimal regulators for nonholonomic systems driven by rough paths. IFAC-PapersOnLine **48**(13), 51–56 (2015)

[34] Nishimura, Y.: Stabilization by unbounded-variation noises. Int. J. Robust Nonlinear Control **26**(18), 4126–4147 (2016)

[35] Nishimura, Y., Tsubakino, D.: Stabilization of nonlinear systems by adding state-dependent rough signals. In: Proc. 2017 IEEE Conference on Control Technology and Applications (CCTA) (2017)

[36] Nishimura, Y.: Rough linearization by one-dimensional rough paths. IFAC-PapersOnLine **51**(13), 320–325 (2018) https://doi.org/10.1016/j.ifacol.2018.07.298 . 2nd IFAC Conference on Modelling, Identification and Control of Nonlinear Systems MICNON 2018

[37] Coron, J.-M.: Control and Nonlinearity. Mathematical Surveys and Monographs, vol. 136. American Mathematical Society, Providence, RI (2007). https://doi.org/10.1090/surv/136

[38] Sontag, E.D.: Mathematical Control Theory: Deterministic Finite Dimensional Systems, 2nd edn. Texts in Applied Mathematics, vol. 6. Springer, New York (1998). https://doi.org/10.1007/978-1-4612-0577-7

[39] Sontag, E.D.: Universal nonsingular controls. Systems and Control Letters **19**(3), 221–224 (1992) https://doi.org/10.1016/0167-6911(92)90116-A

[40] Bullo, F., Lewis, A.D.: Geometric Control of Mechanical Systems. Texts in Applied Mathematics, vol. 49. Springer, New York (2004). A geometric formulation of mechanical control systems with constraints. Contains unified treatment of nonholonomic systems, connections, and Lie algebraic accessibility.

[41] Choset, H., Lynch, K.M., Hutchinson, S., Kantor, G., Burgard, W., Kavraki, L.E., Thrun, S.: Principles of Robot Motion: Theory, Algorithms, and Implementations. MIT Press, Cambridge, MA (2005)

[42] Agrachev, A., Sachkov, Y.: Control Theory from the Geometric Viewpoint. Encyclopaedia of Mathematical Sciences, vol. 87. Springer, Berlin (2004). https://doi.org/10.1007/978-3-662-06404-7 . https://doi.org/10.1007/978-3-662-06404-7

[43] Young, L.C.: An inequality of the Holder type, connected with Stieltjes integration. Acta Math. **67**, 251–282 (1936) https://doi.org/10.1007/BF02401743

[44] Barnsley, M.F.: Fractals Everywhere, 2nd edn. Academic Press, Boston, MA (1988)

[45] Falconer, K.J.: Fractal Geometry: Mathematical Foundations and Applications, 1st edn. John Wiley & Sons, Chichester (1990). Comprehensive treatment of self-similar sets, Hausdorff dimension, and regularity; includes rigorous analysis of the scaling exponents from motif parameters.

[46] Hutchinson, J.E.: Fractals and self similarity. Indiana University Mathematics Journal **30**(5), 713–747 (1981) https://doi.org/10.1512/iumj.1981.30.30055

[47] Hall, J. Marshall: A basis for free Lie rings and higher commutators in free groups. Proc. Amer. Math. Soc. **1**, 575–581 (1950)

[48] Chen, K.-T., Fox, R.H., Lyndon, R.C.: Free differential calculus. IV. The quotient groups of the lower central series. Ann. of Math. (2) **68**, 81–95 (1958)

[49] Dynkin, E.: Calculation of the coefficients of the Campbell–Hausdorff series. Dokl. Akad. Nauk SSSR **57**, 323–326 (1947)

[50] Chen, K.T.: Iterated path integrals and generalized paths. Bull. Am. Math. Soc. **73**, 935–938 (1967) https://doi.org/10.1090/S0002-9904-1967-11858-5

[51] Li, Y., Sauzin, D., Sun, S.: The Baker-Campbell-Hausdorff formula via mould calculus. Lett. Math. Phys. **109**(3), 725–746 (2019) https://doi.org/10.1007/s11005-018-1125-5

[52] Isidori, A.: Nonlinear Control Systems, 3rd edn. Communications and Control Engineering. Springer, London (1995). https://doi.org/10.1007/978-1-84628-615-5 . Standard graduate reference on nonlinear control. Explains input–output linearization, Lie derivatives, and local controllability using Lie brackets.

[53] Jurdjevic, V.: Geometric Control Theory. Cambridge Studies in Advanced Mathematics, vol. 52. Cambridge University Press, Cambridge (1997). https://doi.org/10.1017/CBO9780511530036